Incorporating leaf chlorophyll content into a two-leaf terrestrial biosphere model for estimating carbon and water fluxes at a forest site

Xiangzhong Luo [a*], Holly Croft [a], Jing M. Chen [a], Paul Bartlett [b], Ralf Staebler [c], Norma Froelich [d]

[a] Department of Geography and Planning, University of Toronto, Toronto, ON, M5S 3G3, Canada

[b] Climate Research Division, Environment and Climate Change Canada, Toronto, ON, M3H 5T4, Canada

[c] Air Quality Processes Research Section, Environment and Climate Change Canada, Toronto, ON, M3H 5T4, Canada

[d] Earth, Environmental and Geographical Sciences, Northern Michigan University, Marquette, MI 49855, USA

*Corresponding author

Xiangzhong Luo, email: xiangzhong.luo@mail.utoronto.ca

Abstract

Chlorophyll is the main light-harvesting pigment in leaves, facilitating photosynthesis and indicating the supply of nitrogen for photosynthetic enzymes. In this study, we explore the feasibility of integrating leaf chlorophyll content (Chl_{leaf}) into a Terrestrial Biosphere Model

(TBM), as a proxy for the leaf maximum carboxylation rate at 25°C (V_{max}^{25}), for the purpose of improving carbon and water flux estimation. Measurements of Chl_{leaf} and V_{max}^{25} were made in a deciduous forest stand at the Borden Forest Research Station in southern Ontario, Canada, where carbon and water fluxes were measured by the eddy covariance method. The use of Chl_{leaf}-based V_{max}^{25} in the TBM significantly reduces the bias of estimated gross primary productivity (GPP) and evapotranspiration (ET) and improves the temporal correlations between the simulated and the measured fluxes, relative to the commonly employed cases of using specified constant V_{max}^{25}, leaf area index (LAI)-based V_{max}^{25} or specific leaf area (SLA)-based V_{max}^{25}. The biggest improvements are found in spring and fall, when the mean absolute errors (MAEs) between modelled and measured GPP are reduced from between 2.2-3.2 to 1.8 g C m^{-2} d^{-1} in spring and from between 2.1-2.8 to 1.8 g C m^{-2} d^{-1} in fall. The MAEs in ET estimates are reduced from 0.7-0.8 mm d^{-1} to 0.6 mm d^{-1} in spring, but no significant improvement is noted in autumn. A two-leaf upscaling scheme is used to account for the uneven distribution of incoming solar radiation inside canopies and the associated physiological differences between leaves. We found that modelled V_{max}^{25} in sunlit leaves is 34% larger than in the shaded leaves of the same Chl_{leaf}, which echoes previous physiological studies on light acclimation of plants. This study represents the first case of the incorporation of chlorophyll as a proxy for V_{max}^{25} in a two-leaf TBM at a forest stand and demonstrates the efficacy of using chlorophyll to constrain V_{max}^{25} and reduce the uncertainties in GPP and ET simulations.

Keywords: chlorophyll; photosynthesis; terrestrial biosphere model; evapotranspiration; two-leaf scheme

1. Introduction

Predicting gross primary productivity (GPP) and evapotranspiration (ET) has posed a challenge for accurately quantifying the global terrestrial carbon, water and energy budgets in the context of climate change (Jung et al., 2010; Schaefer et al., 2012). State-of-the-art terrestrial biosphere models (TBMs) have been developed to quantify carbon and water fluxes by describing physical and physiological processes in the soil-vegetation-atmosphere continuum. Model validation and inter-model comparisons have suggested that TBMs are particularly sensitive to the parameterization of leaf photosynthetic capacity (Kattge et al., 2009). Since leaf photosynthetic parameters can only be measured directly at the leaf level (Wilson et al., 2000; Xu and Baldocchi, 2003), using labour-intensive instruments, their limited availability in both space and time has hindered progress in improving GPP and ET estimates by TBMs. Consequently, finding a reliable and easily measurable proxy for leaf photosynthetic parameters across large spatial scales is paramount for the modelling community.

Most TBMs simulate photosynthesis using an enzyme-kinetic model developed by Farquhar (Farquhar et al., 1980). Two key parameters are used to represent the leaf photosynthetic capacity: the maximum carboxylation capacity (V_{max}^{25}) and the maximum electron transport capacity (J_{max}^{25}) at 25°C. V_{max}^{25} refers to the kinetic properties of the enzyme ribulose 1,5-bisphosphate carboxylase/oxygenase (Rubisco) within the Calvin-Benson cycle. J_{max}^{25} is related to the intrinsic properties of the thylakoid membrane, which corresponds to the availability of the cytochrome b6f complex (Cty f) (Hikosaka and Terashima, 1995) to transport electrons in order to produce chemical energy transfers such as ATP and NADPH. ATP and

NADPH are then used to drive the Calvin-Benson Cycle by reducing Rubisco into ribulose bisphosphate (RuBP). On average about two electrons are needed to reduce one unit of Rubisco, implying a constant ratio between J_{max}^{25} and V_{max}^{25}. Frequently, V_{max}^{25} and J_{max}^{25} are each prescribed as a constant value for a given plant functional type (PFT) based on limited measurements (Medlyn et al., 1999; Wullschleger, 1993). Owing to the fact that Rubisco and Cty f are both rich in nitrogen, some studies derived V_{max}^{25} and J_{max}^{25} from a global compilation of nitrogen traits in plants, assuming a linear relationship between Rubisco and leaf nitrogen content per unit area (N_{area}) (Kattge et al., 2009; Walker et al., 2014). However, accurately represented temporal and spatial variations in both V_{max}^{25} and J_{max}^{25} are still elusive as a robust observational methodology to quantify the dynamics of N_{area} across large spatial extents is lacking (Knyazikhin et al., 2013). Moreover, some studies have questioned the efficacy of the nitrogen-based method because the relationship between N_{area} and Rubisco varies temporally due to the dynamic allocation of N_{area} between photosynthetic and non-photosynthetic components in leaves, particularly over a growing season (Croft et al., 2017; Kalacska et al., 2015).

Recent research has drawn attention to the potential of using leaf chlorophyll content (Chl_{leaf}) as an alternative constraint on leaf photosynthetic capacities (Croft et al., 2015a, 2017; Houborg et al., 2013; Koffi et al., 2015; Alton, 2017). Chlorophyll molecules located in light-harvesting-complexes (LHCs) absorb photons, which are then transported to initiate specific redox reactions of chlorophyll molecules in Photosystem II to donate electrons to the electron transport chain (ETC). The concentration of Chl_{leaf} is related to the rate of photosynthesis

through its determining role in the instantaneous electron transport rate (J) (Porcar-Castell et al., 2014). As Chl_{leaf} is a nitrogen rich pigment, Chl_{leaf}, Rubisco and Cty f are linearly related to each other according to their common correlations to the leaf photosynthetic nitrogen pool (Evans, 1989a; Hikosaka and Terashima, 1996; Terashima and Evans, 1988). Recent research has demonstrated that it is possible to model J_{max}^{25} and V_{max}^{25} from Chl_{leaf} using simple linear equations (Houborg et al., 2013; Croft et al., 2017). This potential role of Chl_{leaf} as a proxy for photosynthetic capacity has important implications for improved modelling at regional to global scales, through the ability of estimating Chl_{leaf} from remotely sensed data, using empirical (Croft et al., 2014a; Gitelson et al., 2005; Wu et al., 2008) and physically-based models (Croft et al., 2013; Croft et al., 2015b; Houborg et al., 2015a; Zhang et al., 2007). Satellite-derived Chl_{leaf} will provide an accurate, achievable way of quantifying J_{max}^{25} and V_{max}^{25} in a temporally and spatially explicit manner.

Based on the assumptions above, Houborg et al. (2013) proposed a framework to incorporate measured or satellite-derived Chl_{leaf} into TBMs by building universal Chl_{leaf}– V_{max}^{25} relationships for C3 and C4 plants. Their inclusion of Chl_{leaf} into a TBM helped the GPP simulations to better capture the daily and seasonal variations of observed fluxes over a corn field. Beyond that, limited work has been done to incorporate Chl_{leaf} in TBMs, except for works that have related Chl_{leaf} to vegetation productivity using empirical light use efficiency (LUE) approaches (Croft et al., 2015a; Gitelson et al., 2006; Houborg et al., 2011). As forests account for 50% of the global GPP (Pan et al., 2013) and 45% of the global ET (Oki and Kanae, 2006), there is a growing interest in exploring the potential to use Chl_{leaf}–V_{max}^{25} relationship in forests

111 to improve the prediction of carbon and water fluxes in these areas.

112

113 The complex structures of forest canopies present greater challenges in the upscaling process
114 than for homogenous croplands. Canopy architecture leads to an uneven distribution of solar
115 irradiance from the sunlit top of trees to the shaded interior of a canopy. Values of N_{area} are
116 larger in the sunlit part of the canopy than in shaded leaves, with N_{area} declining from the top
117 to the bottom of a canopy, mimicking the gradient of long-term radiation distribution (Field,
118 1983; Hirose and Werger, 1987; Niinemets, 1997; Warren and Adams, 2001). Along with the
119 changes in N_{area}, the abundance of the nitrogen-rich photosynthetic components -- Rubisco and
120 Cty f -- is reported to be highly correlated to N_{area} and vary from the top to the bottom of the
121 canopy in proportion with N_{area} (Evans, 1989a; Sage et al., 1987). However, Chl_{leaf} is reported
122 to be largely unrelated to the N_{area} gradient and is almost uniform for leaves under various light
123 environments (Anderson et al., 1988; Iio et al., 2005; Lambers et al., 2008; Lichtenthaler et al.,
124 2007; Terashima and Evans, 1988; Walters, 2005), although some studies show a slight
125 chlorophyll gradient (Demarez et al., 1999; Yang et al., 2016; Zhang et al., 2007). These trends
126 lead to a substantially higher Chl_{leaf} : N_{area} ratio in shaded conditions than in full sunlight, which
127 imposes variations on the Chl_{leaf}–V_{max}^{25} relationships inside a canopy. This phenomenon has
128 been attributed to an optimal nitrogen allocation in plants, to maximise the overall productivity
129 of the canopy (Kull, 2002). Accordingly, for shaded leaves, relatively more nitrogen will be
130 allocated to chlorophyll in order to harvest photons, while for sunlit leaves, relatively more
131 nitrogen will be invested in Rubisco and Cty f to accelerate dark reactions (Evans, 1989b;
132 Hikosaka, 2014; Hikosaka and Terashima, 1996).

In this study, a TBM incorporating a two-leaf upscaling scheme is used to estimate GPP and ET within a deciduous forest, across two growing seasons. The two-leaf scheme separates a canopy into groups -- sunlit leaves and shaded leaves -- based on the first-order features of instantaneous solar irradiance on leaves (Chen et al., 1999; Norman, 1982; Sinclair et al., 1976). It is a robust description of the complex leaf light environment in canopies and has been proven to be more capable of simulating GPP and ET variations than the commonly used big-leaf scheme (Chen et al., 1999; De Pury and Farquhar, 1997; Luo et al., in review). The two-leaf scheme delivers an available and potential tool to account for the variations in the Chl_{leaf}–V_{max}^{25} relationship in a complex forest canopy, as well as for other physiological traits affected by the light environment. Using intensive leaf-level and canopy-level measurements at a temperate broadleaf forest, the specific objectives of this study are to:

1) investigate the improvements in GPP and ET simulations from a two-leaf TBM that uses Chl_{leaf} to constrain V_{max}^{25};

2) evaluate the differences in the Chl_{leaf}–V_{max}^{25} relationship, and other physiological traits, between sunlit and shaded leaves.

2.0 Materials and methods

2.1 Site profile

The Borden Forest Research Station is a mixed temperate forest site located in southern Ontario, Canada (44°19'N, 79°56'W) (Froelich et al., 2015). It lies within an ecotone that extends across eastern North America between 44 and 47°N and contains both southern temperate species and

155 northern boreal species. The vegetation at the Borden site is dominated by red maple (*Acer*
156 *rubrum*), eastern white pine (*Pinus strobus*), large-tooth and trembling aspen (*Populus*
157 *grandidentata* and *Populus tremuloides*) and white ash (*Fraxinus americana* (Lee et al., 1999;
158 Teklemariam et al., 2009). The fetch of largely uninterrupted forest extends to distances of 1.5–
159 4 km in the southeastern and southwestern quadrants, and to 1 km in the northeastern direction.
160 The northwestern fetch contains a white pine plantation and was not included in the footprint
161 of eddy-covariance (EC) flux calculations at the site (Froelich et al., 2015). The soil type is
162 sandy loam (Gonsamo et al., 2015). From 2008 to 2013, the average temperature was 8.64℃,
163 precipitation was 808 mm/year and average daytime solar irradiance was 301 W/m2.
164
165 **2.2 Field measurements**
166 Four dominant C3 broadleaf species (red maple, trembling aspen, large-tooth aspen and white
167 ash) were sampled during the growing seasons of 2013, 2014 and 2015. Foliar chlorophyll was
168 measured every 7 to 15 days from five leaf samples per species taken from top-of-canopy
169 branches accessed directly from the 44 m flux tower. Branches were tagged to ensure repeatable
170 sampling throughout the season, and the leaf samples were kept in cool, dark conditions during
171 transport back to a laboratory for analysis. Leaf chlorophyll was extracted using *N,N-*
172 *dimethylformamide*, and was analysed using a Shimadzu UV-1700 Spectrophotometer, with
173 extinction coefficients specified by Wellburn (1994).
174
175 Leaf gas exchange measurements were made on the same days as chlorophyll sampling, using
176 a LI- 6400XT portable infrared gas analyser (LI-COR Inc., Lincoln, NE, USA). CO_2 response

curves (A-Ci curve) of the leaves on the tagged branches were measured under an artificial saturated light source of 1800 μmol photons $m^{-2}s^{-1}$ and stepwise ambient CO_2 concentrations of 400, 200, 100, 50, 400, 400, 600, 800, 1000, 1200, 1500, 1800 ppmv. $V_{max\_0}^{25}$ and $J_{max\_0}^{25}$, the V_{max}^{25} and J_{max}^{25} of the leaves at the top of the canopy, were calculated from the A-Ci curves using a curve-fitting tool developed by Kevin Tu (www.landflux.org) following Ethier and Livingston (2004) and then normalised to 25 °C (Sharkey et al., 2007).

Canopy structural parameters were also collected at 10 m intervals on the same days along a 100 m transect, extending from the flux tower in a North-South orientation. Effective LAI (L_e) values were obtained using the LAI-2000 plant canopy analyser (Li-Cor, Lincoln, NE, USA), while the element clumping index (Ω_E) was measured using the TRAC (Tracing Radiation and Architecture of Canopies) instrument (Chen and Cihlar, 1995). The true LAI time sequences were then calculated as follows (Chen et al., 1999):

$$\mathrm{LAI} = [(1-\alpha)\mathrm{L}_e\gamma_\mathrm{E}]/\Omega_\mathrm{E} \quad (1)$$

where α is the ratio of woody area to total area and γ_E is the ratio of needle area to shoot area. The ratio of woody area to total area (α = 0.17) (Croft et al, 2015a) accounts for the interception of radiation by branches and tree trunks that results in artificially high LAI values, Ω_E is set at 0.95 based on the TRAC measurements. For broadleaf species, individual leaves are considered the foliage elements and γ_E is set at 1.

2.3 Flux and meteorological measurements

The eddy covariance measurements were made at the height of 33 m using a sonic anemometer

(K-Type, Applied Technologies Inc., USA) coupled with a closed-path infrared gas analyzer (IRGA, model LI-6262, LI-COR Biosciences, USA) which is located in a temperature-controlled hut at the base of the tower. Both the IRGA and anemometer are operated at 10 Hz. High frequency eddy covariance fluxes were processed and aggregated into half-hourly fluxes using the method described in Froelich et al. (2015).

The half-hourly net ecosystem exchange (NEE, μmol $m^{-2}s^{-1}$) is calculated as $-(F_c+S_c)$, where F_c is the covariance between vertical wind velocity (w') and atmospheric CO_2 concentration (c'). S_c is the rate of change of CO_2 storage per unit ground area in the air layer below the EC sensors. F_c was calculated from the WPL(Webb-Pearman-Leuning)-corrected vertical turbulent transport of the CO_2 mole fraction as $F_c = \rho_a \overline{w' c'_{WPL}} / M_a$, where the WPL accounts for density effects due to water vapor fluctuations (Webb et al., 1980), ρ_a is the density of air and M_a is the molecular weight of dry air. The storage change S_c was estimated as $S_c = \int_0^{Z_{ec}} \frac{\Delta CO_2}{\Delta t} dz$, where Z_{ec} is the height of the EC sensors at 33m and t refers to time. Other terms such as horizontal advection are assumed to be negligible. NEE data were then filtered during periods of low turbulence (Staebler and Fitzjarrald, 2004) and when winds were from the direction of the short fetch (i.e. wind direction was >285° or <20°) (Froelich et al., 2015). A change point detection method (Barr et al., 2013) was used to derive the friction velocity threshold (u*) to identify periods suitable for the application of the eddy covariance method to calculate fluxes. Gaps in the NEE data were filled using the method of Barr et al. (2004). During nights or cold periods respiration (RE) was simply computed as $RE = NEE$, while during warm periods or in cases of data gaps, RE was estimated using an empirical model based on air and soil temperature (Froelich et al., 2015). Half-hourly GPP was then calculated as $GPP =$

221 $NEE + RE$; gaps in GPP were filled with an empirical model based on PAR (Barr et al., 2004;
222 Froelich et al., 2015).
223
224 In conjunction with the CO_2 flux measurements, the EC system also measured the latent heat
225 flux (LE, W m^{-2}) as $LE = L\rho_a\overline{w'q'_{WPL}}$, where L is the latent heat of vaporization (kJ g^{-1}), ρ_a
226 is the density of air (kg m^{-3}) and $\overline{w'q'_{WPL}}$ is the WPL-corrected covariance between the
227 vertical wind velocity and atmospheric water vapor mixing ratios (m s^{-1} mol H_2O mol^{-1} air).
228 (Froelich et al., 2015; Teklemariam et al., 2009). Gaps in the LE measurements were not filled.
229
230 Several half-hourly auxiliary microclimate variables were also collected at the site to initialize
231 and force the TBM. Wind speed (m s^{-1}) and wind direction were measured by the sonic
232 anemometer mounted at the height of 33 m. Continuous air temperature (°C) and relative
233 humidity (%) were measured at various heights, but the 33 meter data were selected as model
234 inputs. Incoming solar irradiance on the canopy was measured at the top of the flux tower
235 (Froelich et al., 2015). Soil moisture (m^3 m^{-3}) measured at the depth of 5 cm to 30 cm was used.
236 Precipitation data (mm h^{-1}) were obtained from the nearest Environment Canada weather
237 station that has hourly rainfall records (ID: Borden AWO), which is approximately 5.2 km away.
238
239 **2.4 Terrestrial biophysical model**
240 The Boreal Ecosystem Productivity Simulator (BEPS) is a two-leaf enzyme-kinetic model
241 initially developed to estimate the carbon uptake and the water cycle of boreal ecosystems
242 (Chen et al., 1999; Liu et al., 2003). It has been substantially upgraded since its original release

to simulate carbon and water fluxes at an hourly time step over various PFTs (Chen et al., 2007; Ju et al., 2006). Several inter-model comparisons and site-level validations have shown that BEPS can produce reliable GPP and ET estimates (Amthor et al., 2001; Potter et al., 2001; Grant et al., 2006; Gonsamo et al., 2013). The modules related to the utilization of Chl_{leaf} in BEPS are described in the following subsections.

2.4.1 Separation of sunlit and shaded leaves.

The two-leaf scheme is an abstraction of the instantaneous radiation regime in canopies. Leaves are separated into sunlit leaves and shaded leaves based on illumination and canopy geometry. Sunlit leaves tend to be light saturated because they receive both direct and diffuse solar radiation, while shaded leaves only receive diffuse radiation (Appendix A). The values of $\mathrm{LAI_{sunlit}}$ and $\mathrm{LAI_{shaded}}$ are calculated following the stratification scheme of Norman (1982) and Chen et al. (1999):

$$\mathrm{LAI_{sunlit}} = 2\cos\theta(1 - \exp(-0.5\Omega\mathrm{LAI_{tot}}/\cos\theta)) \quad (2)$$

$$\mathrm{LAI_{shaded}} = \mathrm{LAI_{tot}} - \mathrm{LAI_{sunlit}} \quad (3)$$

where θ is the solar zenith angle, $\mathrm{LAI_{tot}}$ is the total leaf area index of the canopy, and Ω is the clumping index of this site, where $\Omega = \Omega_E/\gamma_E$.

2.4.2 Derivation of $\mathbf{V_{max}^{25}}$ and $\mathbf{J_{max}^{25}}$ for sunlit and shaded leaves

In BEPS, $V_{max\_0}^{25}$ is the input parameter to quantify the leaf photosynthetic capacity. The V_{max}^{25} values for sunlit and shaded leaves are each derived respectively based on the $V_{max\_0}^{25}$ value, the vertical nitrogen profile of the canopy, the fraction of sunlit and shaded leaves and (Chen

et al., 2012).

Leaf nitrogen content per unit leaf area $N(L)$ (g m^{-2}) generally decreases exponentially from the top to the bottom in a canopy following the long-term radiation distribution in the canopy (Equation 4):

$$N(L) = N_0 e^{-k_n L} \quad (4)$$

where the extinction coefficient $k_n = 0.3$ (De Pury and Farquhar, 1997), N_0 is the nitrogen content of leaves at the top-of-canopy, and L is the canopy depth expressed as LAI from the top to a given height. V_{max}^{25} is proportional to the leaf nitrogen content, and therefore it could be expressed as:

$$V_{max}^{25}(L) = V_{max\_0}^{25} \chi_n N(L) \quad (5)$$

where $V_{max\_0}^{25}$ is the V_{max}^{25} of leaves at the top-of-canopy, and χ_n (m^2 g^{-1}) quantifies the relative change of V_{max}^{25} to the leaf nitrogen content in the canopy, while $N(L)$ has the unit of g/m^2. The value of χ_n, the mean value of N_{area} and its standard deviation, and the standard deviation of V_{max}^{25} are provided for each PFT (Chen et al., 2012; Kattge et al., 2009); we have only used the values for deciduous broadleaf forests in this study. Since we do not have records specifically for N_0, N_0 is regarded as the sum of the mean N_{area} and its standard deviation, which are provided by Kattge et al. (2009). Using Equation 4 and 5 and our estimated N_0, we can quantify the vertical patterns of V_{max}^{25} in the canopy.

The fractions of sunlit (f_{sun}) and shaded leaves (f_{sh})in the canopy change with the canopy depth:

$$f_{sun}(L) = \Omega e^{-kL} \quad (6)$$

$$f_{sh}(L) = 1 - \Omega e^{-kL} \quad (7)$$

where $k = G(\theta)\Omega/\cos\theta$. The projection coefficient of the canopy, $G(\theta)$, is taken as 0.5 assuming a spherical leaf angle distribution. We assume that V_{max}^{25} of a representative sunlit or shaded leaf is equal to the mean V_{max}^{25} value of the sunlit or shaded leaf group. Therefore, the V_{max}^{25} of a representative sunlit or shaded leaf is expressed through the following integrations:

$$V_{max\_sunlit}^{25} = \frac{\int_0^L V_{max\_0}^{25}\chi_n N(L) f_{sun}(L)dL}{\int_0^L f_{sun}(L)dL} = V_{max\_0}^{25}\chi_n N_0 \frac{\int_0^L e^{-k_n L}\Omega e^{-kL}dL}{\int_0^L \Omega e^{-kL}dL} = V_{max\_0}^{25}\chi_n N_0 \frac{k[1-e^{-(k_n+k)L}]}{(k_n+k)(1-e^{-kL})} \quad (8)$$

$$V_{max\_shaded}^{25} = \frac{\int_0^L V_{max\_0}^{25}\chi_n N(L) f_{sh}(L)dL}{\int_0^L f_{sh}(L)dL} = V_{max\_0}^{25}\chi_n N_0 \frac{\int_0^L e^{-k_n L}(1-\Omega e^{-kL})dL}{\int_0^L (1-\Omega e^{-kL})dL} = V_{max\_0}^{25}\chi_n N_0 \frac{\frac{1}{k_n}(1-e^{-k_n L}) - \frac{\Omega}{k+k_n}[1-e^{-(k_n+k)L}]}{L-2\cos\theta(1-e^{-kL})} \quad (9)$$

Several methods for estimating $V_{max\_0}^{25}$ are described in Section 2.5. J_{max}^{25} for sunlit and shaded leaves are subsequently obtained using the V_{max}^{25}:J_{max}^{25} built on our in-situ measurements (see Section 2.5).

2.4.3 Simulation of GPP and ET

BEPS calculates the instantaneous GPP as the sum of the photosynthesis from the sunlit leaves and the shaded leaves (Equation 10). Within each sunlit and shaded leaf group, all leaves are assumed to have the same physiological features; photosynthesis of a leaf group is then predicted using one representative leaf multiplied by LAI.

$$GPP = A_{sunlit} \times LAI_{sunlit} + A_{shaded} \times LAI_{shaded} \quad (10)$$

where A_{sunlit} and A_{shaded} are the instantaneous photosynthetic rates of a representative

sunlit leaf and a representative shaded leaf, respectively. Following the Farquhar biochemical model, the instantaneous leaf photosynthetic rate in BEPS (Chen et al., 1999) is described as:

$$A = \min(W_c, W_j) - R_d \quad (11)$$

where W_c is the rate of gross photosynthesis (μmol $m^{-2}s^{-1}$) when RuBP carboxylase/oxygenase is saturated, and W_j is the photosynthetic rate when RuBP-regeneration is limited by electron transport. R_d is the dark respiration rate of CO_2 exchange.

$$W_C = V_{max}\frac{C_i - \Gamma}{C_i + K} \quad (12)$$

$$W_j = J\frac{C_i - \Gamma}{4C_i + 8K} \quad (13)$$

$$R_d = 0.015V_{max} \quad (14)$$

where V_{max} is the maximum carboxylation rate (μmol $m^{-2}s^{-1}$) acquired from the prescribed V_{max}^{25} and a temperature dependent function (Sharkey et al., 2007), J is the electron transport rate (μmol $m^{-2}s^{-1}$). C_i is the intercellular CO_2 concentration (μmol mol^{-1}), and Γ is the CO_2 compensation point in the absence of dark respiration (μmol mol^{-1}), K is a function of Rubisco enzyme kinetics described as $K_c/(1 + O_i/K_o)$, where K_c and K_o are Michaelis–Menten constants for CO_2 (μmol mol^{-1}) and O_2 (mmol mol^{-1}) and O_i is the intercellular oxygen concentration (mmol mol^{-1}). The electron transport rate, J, is a function of the incoming photosynthetic photon flux density (PPFD in μmol $m^{-2}s^{-1}$) and the maximum electron transport (J_{max}):

$$J = J_{max}PPFD/(PPFD + 2.1J_{max}) \quad (15)$$

Following a revised Ball-Woodrow-Berry equation (Ju et al., 2006), leaf stomatal conductance is quantified as:

$$g_s = f_w\left(\frac{mA \cdot RH}{C_s}\right) + g_0 \quad (16)$$

where m is the dimensionless Ball-Woodrow-Berry coefficient set as 8, RH is the relative humidity (%), C_s is the CO_2 concentration on the leaf surface, g_0 is the minimum conductance during the night, and A is the rate of photosynthesis (μmol $m^{-2}s^{-1}$) of the representative sunlit or shaded leaf. The added f_w variable is noted as the soil water stress factor (Appendix B).

After obtaining g_s, leaf-level transpiration is calculated by employing the Penman-Monteith equation in BEPS (Chen et al., 2007):

$$T = \frac{\Delta(R_n - G) + \rho c_p VPD g_v}{\Delta + \left(1 + \frac{g_v}{g_s}\right)\gamma} \times \frac{1}{\lambda} \quad (17)$$

where λ is the latent heat of water (J kg^{-1}), R_n is the instantaneous net radiation on the leaf surface (W/m^{-2}) ((Appendix A), G is the heat storage of the leaf which is a minimum close to 0 (W/m^{-2}), ρ is the density of air (kg m^{-3}), c_p is the specific heat of air (J kg^{-1} °C^{-1}), VPD is the vapor pressure deficit on the surface of a leaf (kPa), γ is the psychrometric constant (kPa °C^{-1}), g_V is the leaf boundary-layer resistance to water vapor (m s^{-1}), and Δ is the derivative of saturated vapor pressure with respect to the air temperature (kPa °C^{-1}). The leaf-level transpiration (mm s^{-1}) is upscaled to the canopy-level transpiration following an analogous protocol to the GPP upscaling.

$$T = T_{sunlit} \times LAI_{sunlit} + T_{shaded} \times LAI_{shaded} \quad (18)$$

where T_{sunlit} is the transpiration from a sunlit leaf and T_{shaded} is the transpiration from a shaded leaf.

In addition to transpiration, BEPS also simulates evaporation from soil and from wet leaves

353 (Chen et al., 2007). These processes are not regulated by stomata and therefore are less likely
354 to be affected by the improvement in V_{max}^{25} parameterization.
355
356 **2.5 Modelling treatments**
357 Empirical equations were developed to relate Chl_{leaf} to $V_{max\_0}^{25}$ and $J_{max\_0}^{25}$, based on field
358 measurements (Croft et al., 2017) and were incorporated into BEPS for the purpose of
359 improving GPP and ET simulations. In order to evaluate the improvements associated with
360 utilising Chl_{leaf} (Case 4), we used three commonly employed $V_{max\_0}^{25}$ treatments as reference
361 cases (Case 1,2 and 3).
362
363 **Case 1:** constant $V_{max\_0}^{25}$. Groenendijk et al. (2011) assimilated eddy covariance measurements
364 from Fluxnet into an inverse model of photosynthesis and transpiration to derive site-specific
365 V_{max}^{25} and PFT-specific V_{max}^{25}. Several BEPS studies have successfully used this set of V_{max}^{25}
366 values for site-level GPP and ET simulations (Gonsamo et al., 2013; Chen et al., 2016; Luo et
367 al., 2017, in review).
368 In this case, we used the value of 62 μmol m^{-2} s^{-1} for temperate deciduous broadleaf forest from
369 Groenendijk et al. (2011) as the constant $V_{max\_0}^{25}$ at the Borden Forest site. This value is
370 comparable to another commonly cited value of 57.7 μmol m^{-2} s^{-1} for deciduous broadleaf
371 forests reported by Kattge et al. (2009).
372
373 **Case 2:** LAI-based $V_{max\_0}^{25}$. Some studies have found that seasonal patterns of V_{max}^{25} follow
374 the seasonal patterns of LAI. We used a scheme developed by Ryu et al. (2011) to calculate

375 $V_{max\_0}^{25}$ on any given day during the growing season:

376 $$V_{max\_0}^{25} = aV_{max\_ref}^{25} + (1-a)V_{max\_ref}^{25}\frac{L_c - L_{min}}{L_{max} - L_{min}} \quad (19)$$

377 where L_{max}, L_{min} and L_c are maximum, minimum and current LAI values over the year.
378 $V_{max\_ref}^{25}$ is the value of maximum V_{max}^{25} during the growing season, which is regarded as 62
379 μmol m^{-2} s^{-1}. The empirical variable a is set at 0.3 as in Ryu et al. (2011). The ratio component
380 $\frac{L_c - L_{min}}{L_{max} - L_{min}}$ ranges between 0 and 1.

381

382 **Case 3:** SLA-based $V_{max\_0}^{25}$. The specific leaf area (SLA) of leaves at the canopy top is used
383 in the Community Land Model version 4.0 (CLM4) to parameterize $V_{max\_0}^{25}$ (Thornton and
384 Zimmermann, 2007). In this case:

385 $$V_{max\_0}^{25} = N_{area} F_{LNR} F_{NR} \alpha_{R25} f(N) \quad (20)$$

386 where N_{area} is the area-based leaf nitrogen concentration (g N m^{-2}), $F_{LNR} = 0.09$ is the
387 fraction of leaf nitrogen in Rubisco (g N in Rubisco g^{-1} N) for temperate broadleaf deciduous
388 trees, $F_{NR} = 7.16$ is the mass ratio of total Rubisco molecular mass to nitrogen in Rubisco (g
389 Rubisco g^{-1} N in Rubisco), and $\alpha_{R25} = 60$ is the specific activity of Rubisco (μmol CO_2 g^{-1}
390 Rubisco s^{-1}). A scaling factor, $f(N) = 0.64$, represents the effects of N limitation. N_{area} is
391 calculated from mass-based leaf N concentration and SLA.

392 $$N_{area} = \frac{1}{CN_L SLA} \quad (21)$$

393 where $CN_L = 25$ is the leaf carbon-to-nitrogen ratio (g C g^{-1} N) for broadleaf trees and SLA
394 is specific leaf area (m^2 g^{-1} C).

395

396 **Case 4:** Chl_{leaf}-based $V_{max\_0}^{25}$. A straightforward way to implement Chl_{leaf} into TBMs is through

a robust relationship between Chl_{leaf} and the photosynthetic parameters (i.e. V_{max}^{25} and J_{max}^{25}). Croft et al. (2017) found a significant linear relationship between Chl_{leaf} and $V_{max\_0}^{25}$ (r^2=0.76, p<0.001) for the four deciduous species at the Borden site with an intercept close to zero (Equation 22 and 23).

$$V_{max\_0}^{25} = 1.3 \times Chl_{leaf} + 3.72 \quad (22)$$

$$J_{max\_0}^{25} = 1.85 \times V_{max\_0}^{25} + 6.87 \quad (23)$$

For leaves at the top of the canopy, an increase of 1 μg cm^{-2} of Chl_{leaf} corresponds to 1.3 μmol m^{-2} s^{-1} in $V_{max\_0}^{25}$. $V_{max\_0}^{25}$ and $J_{max\_0}^{25}$ are significantly related (r^2=0.91, p<0.001) by an empirical equation across four species (Figure 1).

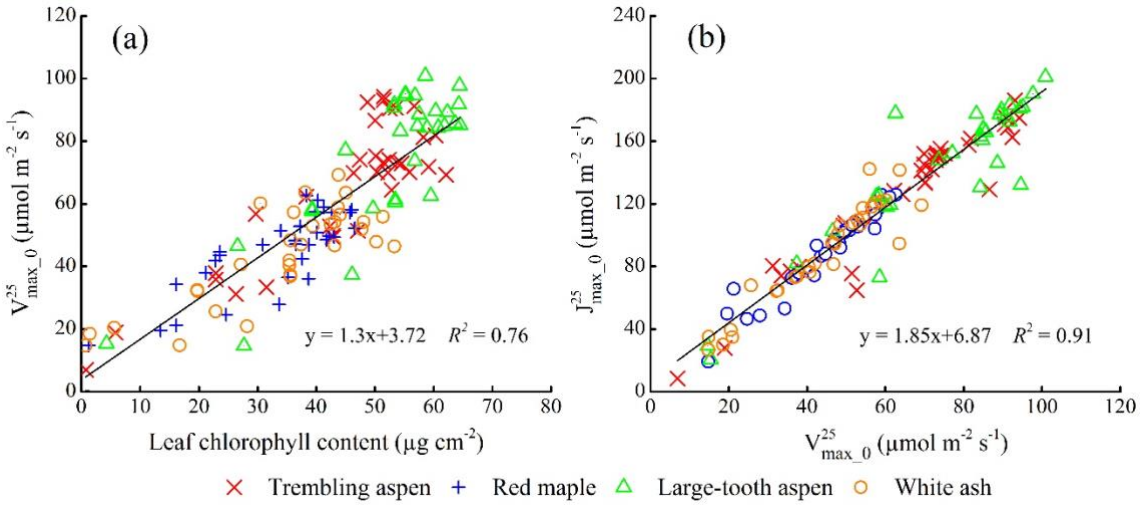

Figure 1. Scatter plots of the measured leaf-level physiological parameters of C3 broadleaf leaves at the top of canopy at the Borden site in 2014 and 2015. (a) $V_{max\_0}^{25}$ versus Chl_{leaf}; (b) $J_{max\_0}^{25}$ versus $V_{max\_0}^{25}$. Source: Croft et al., 2017.

While the ranges of Chl_{leaf}, $V_{max\_0}^{25}$ and $J_{max\_0}^{25}$ each differ among the four species, the linear

414 equations in Figure 1 fit the data points consistently, implying that it is reasonable to use a
415 single equation to link Chl_{leaf} and $V_{max\_0}^{25}$ for broadleaf species. These two equations were used
416 to incorporate Chl_{leaf} into BEPS in Case 4.
417
418 **3. Results**
419 **3.1 Leaf traits and canopy fluxes**
420 Figure 2 shows the variations of Chl_{leaf}, LAI and SLA that are used to constrain $V_{max\_0}^{25}$ in the
421 four modelling cases (Figure 2a), along with simulated V_{max}^{25} and canopy flux measurements
422 (Figure 2b) across two growing seasons. Chl_{leaf}, LAI and SLA were measured every 7-15 days
423 during the two growing seasons; values between the sampling dates were determined by linear
424 interpolation. The Chl_{leaf} and SLA values were calculated based on the weighted composition
425 of the major tree species at the Borden Forest (Teklemariam et al., 2009).

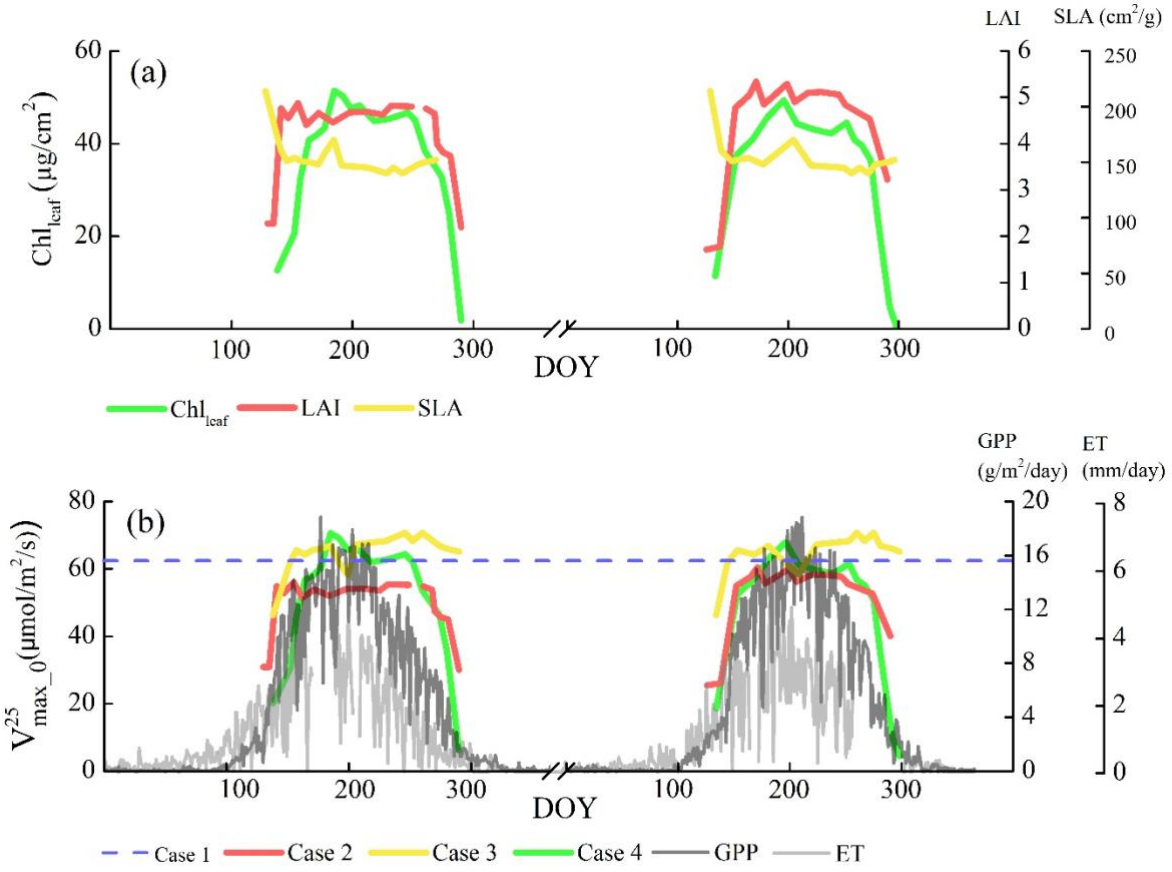

Figure 2. Seasonal variations of (a) Chl_{leaf}, leaf area index (LAI), specific leaf area (SLA), and; (b) simulated $V_{max\_0}^{25}$ for each modelling scenario where: Case 1 (a constant $V_{max\_0}^{25}$), Case 2 (LAI-based $V_{max\_0}^{25}$), Case 3 (SLA-based $V_{max\_0}^{25}$) and Case 4 (Chl_{leaf}-based $V_{max\_0}^{25}$), alongside GPP and ET tower measurements, during 2013 and 2014 at the Borden Forest field site.

In 2013 and 2014, Chl_{leaf} accumulated slowly, beginning in early May, reached its peak in July, with values ranging from 0.6 to 51.4 μg cm-2. In contrast, leaves became fully expanded in a shorter time-frame (over 2 weeks in early-mid May), giving a steeper gradient in the early growing season LAI values. SLA decreased promptly at the beginning of growing seasons and stayed relatively constant from May to October. At the end of the growing season, the

breakdown of chlorophyll began to exceed production in late August, while leaf fall did not begin until October (Croft et al., 2014).

Among the four cases, the simulated Chl_{leaf}-based $V_{max\_0}^{25}$ (Case 4) appears to most closely follow the seasonal variations in measured GPP and ET (Figure 2b). In the modelled scenarios, simulated $V_{max\_0}^{25}$ ranges from: Case 2 - 30.1 to 60.5 μmol m^{-2} s^{-1}; Case 3 - 35 to 70.2 μmol m^{-2} s^{-1}; and Case 4 - 4.4 to 70.6 μmol m^{-2} s^{-1}. Values of $V_{max\_0}^{25}$ from these modelling cases are used in BEPS to simulate GPP and ET over two growing seasons at the Borden Forest.

3.2 Validation of the GPP and ET estimates from different $V_{max\_0}^{25}$ constraints

The simulated GPP and ET results are shown for the four different modelling cases, in order to investigate the effects of the different biophysical constraints on $V_{max\_0}^{25}$. Figure 3 shows linear regressions between the hourly measured fluxes and the hourly estimated fluxes from BEPS.

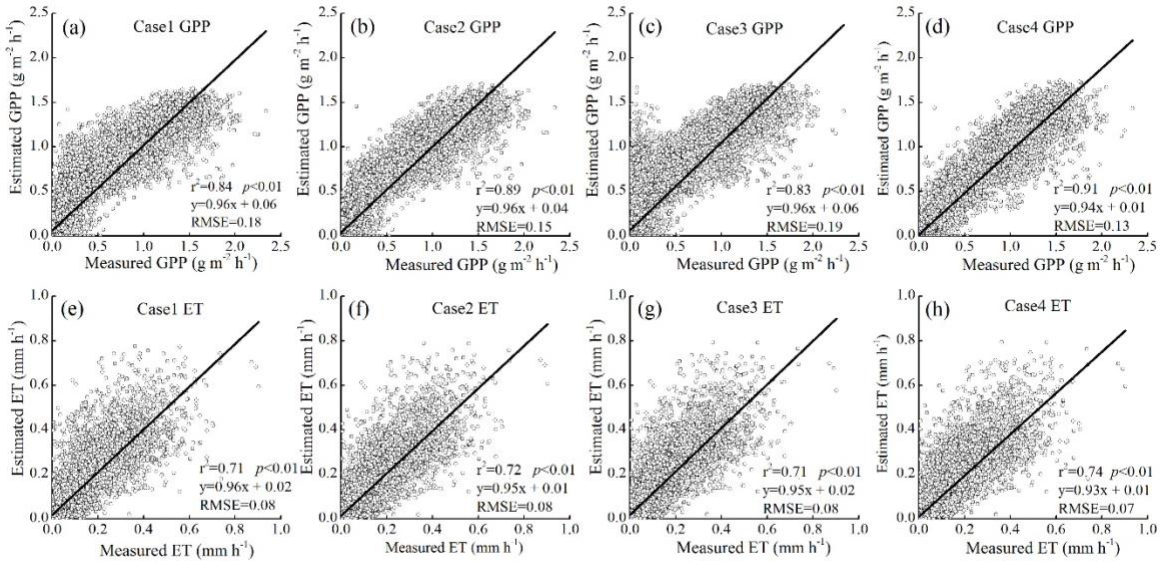

Figure 3. Scatter plots of the predicted and measured fluxes of 2013-2014 at the Borden site.

(a) to (d) refer to the GPP validation in Case 1 (a constant $V_{max\_0}^{25}$), Case 2 (LAI-based $V_{max\_0}^{25}$), Case 3 (SLA-based $V_{max\_0}^{25}$) and Case 4 (Chl_{leaf}-based $V_{max\_0}^{25}$), respectively; (e) to (h) refer to the ET validation in Case 1, Case 2, Case 3 and Case 4, respectively.

Modelled results from Case 4 (Chl_{leaf}-based $V_{max\_0}^{25}$) show the strongest correlation ($r^2 = 0.91$) with measured GPP values, and the lowest RMSE of 0.13 g m^{-2} h^{-1} (Figure 3). The other three modelled scenarios reveal overestimated results at lower GPP values, which likely correspond to the start and the end of the growing season. Additionally, Case 1 (a constant $V_{max\_0}^{25}$) shows underestimations at higher measured GPP values. The total simulated annual GPP values are 2123 g m^{-2} y^{-1}, 1967 g m^{-2} y^{-1}, 2124 g m^{-2} y^{-1} and 1729 g m^{-2} y^{-1} for Case 1 (a constant $V_{max\_0}^{25}$), Case 2 (LAI-based $V_{max\_0}^{25}$), Case 3 (SLA-based $V_{max\_0}^{25}$) and Case 4 (Chl_{leaf}-based $V_{max\_0}^{25}$), respectively, while the annual GPP obtained from flux-tower measurements is 1719 g m^{-2} y^{-1}. The bias of the estimated annual GPP from Case 4 accounts for only 0.6% of observed annual GPP, while the biases from Cases 1, 2 and 3 account for 23.5%, 14.4% and 23.6%, respectively.

The Chl_{leaf} -constrained $V_{max\_0}^{25}$ also produces the strongest relationship between estimated and measured ET ($r^2 = 0.74$; RMSE = 0.07 mm h^{-1}). As with the GPP results, the estimated annual ET for Case 4 of 362 mm y^{-1} is closest to the measurement value of 370 mm y^{-1}, while the other annual ET results are 414 mm y^{-1} (Case 1), 397 mm y^{-1} (Case 2), 409 mm y^{-1} (Case 3). The bias of the estimated annual ET from Case 4 accounts for -2.2% of measured annual ET, while to the biases from Case 1, 2 and 3 account for 11.9%, 7.3% and 10.5% of the annual

observed ET. Overall, Case 4 is the most accurate scenario for simulating both total amount and temporal variations of carbon and water fluxes.

3.3 Seasonality of the improvements in estimated GPP and ET

In order to investigate the seasonal variability in the improvements made to GPP and ET estimations using Case 4 relative to Cases 1-3 (Figure 3), the monthly mean absolute errors (MAEs) and the relative MAEs of the modelled fluxes are shown for the four cases (Figure 4). .

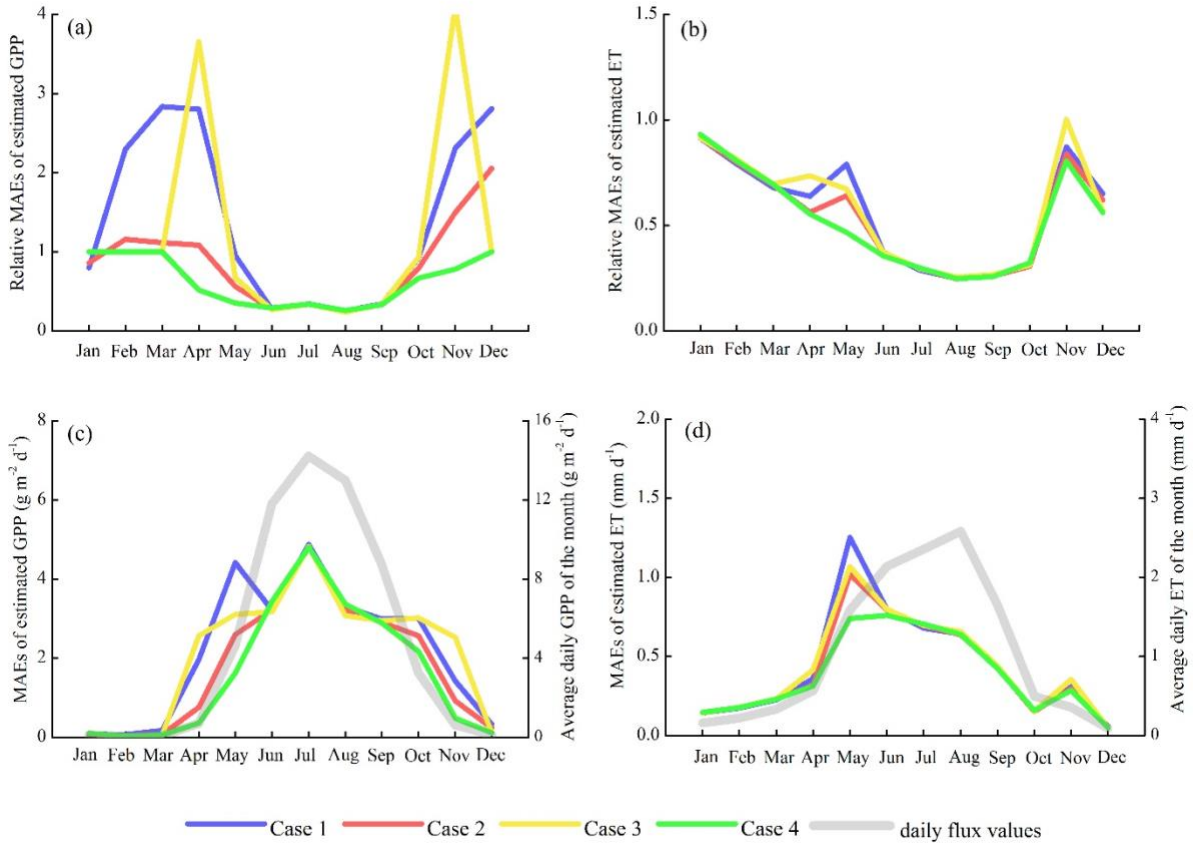

Figure 4. The monthly relative MAEs (a, b) and the MAEs (c, d) between the estimated and measured daily fluxes in 2013-2014, under the four modelling cases. (a, c) GPP and (b, d) ET.

The relative MAEs are the division of MAEs by daily flux values.

Figure 4a and 4b shows that Case 4 introduces the smallest errors in most months for both GPP and ET estimates. Other cases display larger MAEs and relative MAEs than Case 4, especially at the beginning and end of the growing seasons. In Figures 4c and 4d, the average MAEs of estimated GPP in spring (from April to June) of the four cases are 3.2 g m^{-2} d^{-1}, 2.2 g m^{-2} d^{-1}, 3.0 g m^{-2} d^{-1} and 1.8 g m^{-2} d^{-1} respectively; in autumn (from September to November), the average MAEs of estimated GPP for the four cases are 2.4 g m^{-2} d^{-1}, 2.1 g m^{-2} d^{-1}, 2.8 g m^{-2} d^{-1} and 1.8 g m^{-2} d^{-1}, respectively. In the middle of the growing seasons, the improvements are not pronounced since the V_{max}^{25} values derived from all cases are close to each other. The major improvements in modelled ET also appear in spring (from April to June), where the MAEs are reduced from 0.8 mm d^{-1} in Case 1, 0.7 mm d^{-1} in Case 2 and 0.8 mm d^{-1} in Case 3 to 0.6 mm d^{-1} in Case 4. In fall (from September to November), small improvements on the order of 0.01 mm d^{-1} in MAEs are observed from Case 1, 2 and 3 to Case 4. From June to August, the ET estimates show little differences among the four cases.

3.4 Assessing the relative contribution of Chl_{leaf} to modelled GPP and ET

According to the modelling results, Chl_{leaf} -V_{max}^{25} markedly improved the estimation of GPP and ET during the transitional periods of the growing season. However, the improvement in ET is not as great as the improvement in GPP (Figure 4). This decoupling effect of carbon and water fluxes suggests that there are differences in the sensitivities of GPP and ET to the forcing variables. In Figure 5, we explored the sensitivities of GPP and ET to five forcing variables of

BEPS: incoming solar radiation (R_s), air temperature (T_{air}), relative humidity (RH), LAI and Chl_{leaf}. To assess the sensitivity of GPP and ET to certain variables, each variable was changed by -20%, -10%, 10% and 20% stepwise to drive BEPS (Case 4), while all other variables remained unchanged. The resulting changes in simulate GPP and ET were recorded and analyzed.

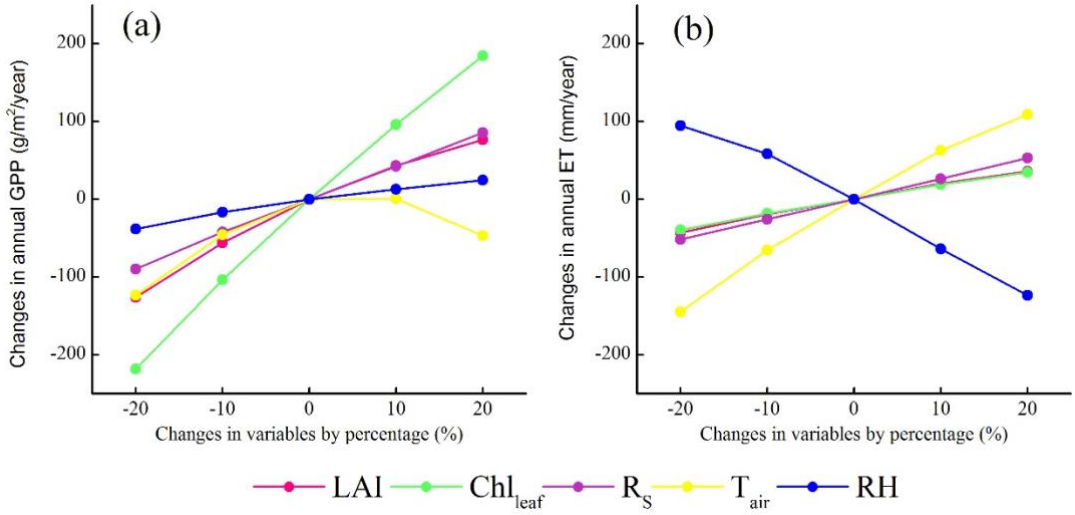

Figure 5. Sensitivity of GPP and ET to the incoming solar radiation (R_s), air temperature (T_{air}), relative humidity (RH), LAI and Chl_{leaf} at the Borden site. (a) GPP; (b) ET.

Figure 5a shows that GPP is most sensitive to the changes in Chl_{leaf}. A 20% variation in Chl_{leaf} leads to a change in annual GPP as large as 200 g m^{-2} y^{-1}. In addition to Chl_{leaf}, R_s and LAI are linearly linked to GPP with similar order of importance. There is an optimal T_{air} range for GPP, with higher or lower T_{air} damping the carbon assimilation rate. RH has the least influence on GPP. In contrast, ET is most sensitive to the climatic variables, T_{air} and RH, whilevariables used to describe the plant functional status (i.e. LAI and Chl_{leaf}) drive smaller changes in ET (Figure 5b). As such, the variation in ET resulting from the changing Chl_{leaf} and LAI in spring

and autumn is overshadowed by the variation from changing temperature and humidity. Consequently, ET is less improved than GPP by incorporating Chl_{leaf} based V_{max}^{25} in the TBM.

3.5 The impact of light environment within the canopy on leaf physiology

This study incorporates Chl_{leaf} into a two-leaf model to consider the complex light environment in forests and the accompanying physiological traits of sunlit and shaded leaves. Light intensity within the canopy affects the relative allocation of nitrogen between light-harvesting chlorophyll molecules and Rubisco in the Calvin cycle. Consequently, it is important to consider how this dynamic partitioning of nitrogen affects the integration of chlorophyll into the two-leaf BEPS model, and how this partitioning impacts carbon and water exchange. Figure 6 shows the contrasting modelled solar irradiance for sunlit and shaded leaves over the two growing seasons.

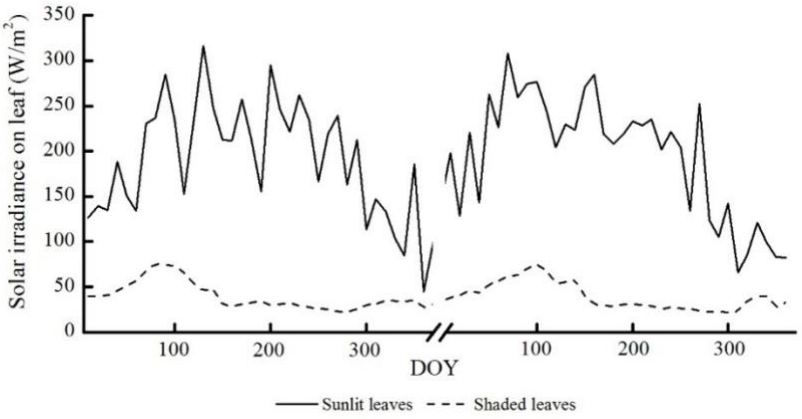

Figure 6. Seasonal patterns of the average daily incoming solar radiation (W/m2) on sunlit and shaded leaves simulated by BEPS in 2013 and 2014.

The daytime average solar radiation on sunlit leaves ranges from 105 to 316 W m-2 from DOY 100 to DOY 300, with an average value of 216 W m-2. In contrast, the solar irradiance on

shaded leaves ranges from 22 to 75 W m^{-2} in the same period, with an average of 36 W m^{-2}. This 6-fold difference in the light environment results in a different role of chlorophyll between the sunlit and shaded leaves, as shown in Figure 7.

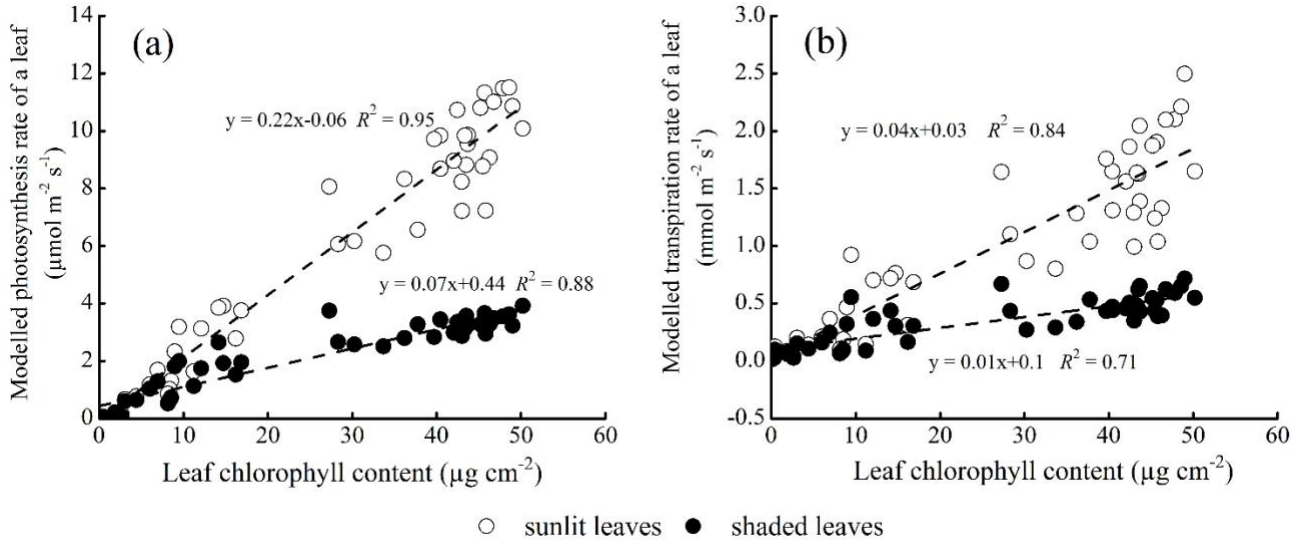

Figure 7. BEPS modelled leaf photosynthesis and transpiration rates and their relationship to Chl_{leaf}. Sunlit (open dots) and shaded leaves (solid dots) are compared. Ten-day averages of the modelled photosynthesis and transpiration rates in the growing seasons are used.

For modelled sunlit leaves, an increase of 1 μg cm^{-2} in Chl_{leaf} increases the rate of photosynthesis by 0.22 μmol m^{-2} s^{-1} and the rate of transpiration by 0.04 mmol m^{-2} s^{-1} in sunlit leaves. In contrast, photosynthesis and transpiration of shaded leaves are less sensitive to changes in Chl_{leaf}:a 1 μg cm^{-2} increase in Chl_{leaf} leads to only a 0.07 μmol m^{-2} s^{-1} increase in photosynthesis and a 0.01 mmol m^{-2} s^{-1} increase in transpiration of shaded leaves. Importantly, Figure 7 suggests that chlorophyll plays a lesser role in determining GPP and ET in shaded leaves than in sunlit leaves. In line with the different role of chlorophyll, sunlit and shaded leaves shows differences in other physiological traits (Figure 8).

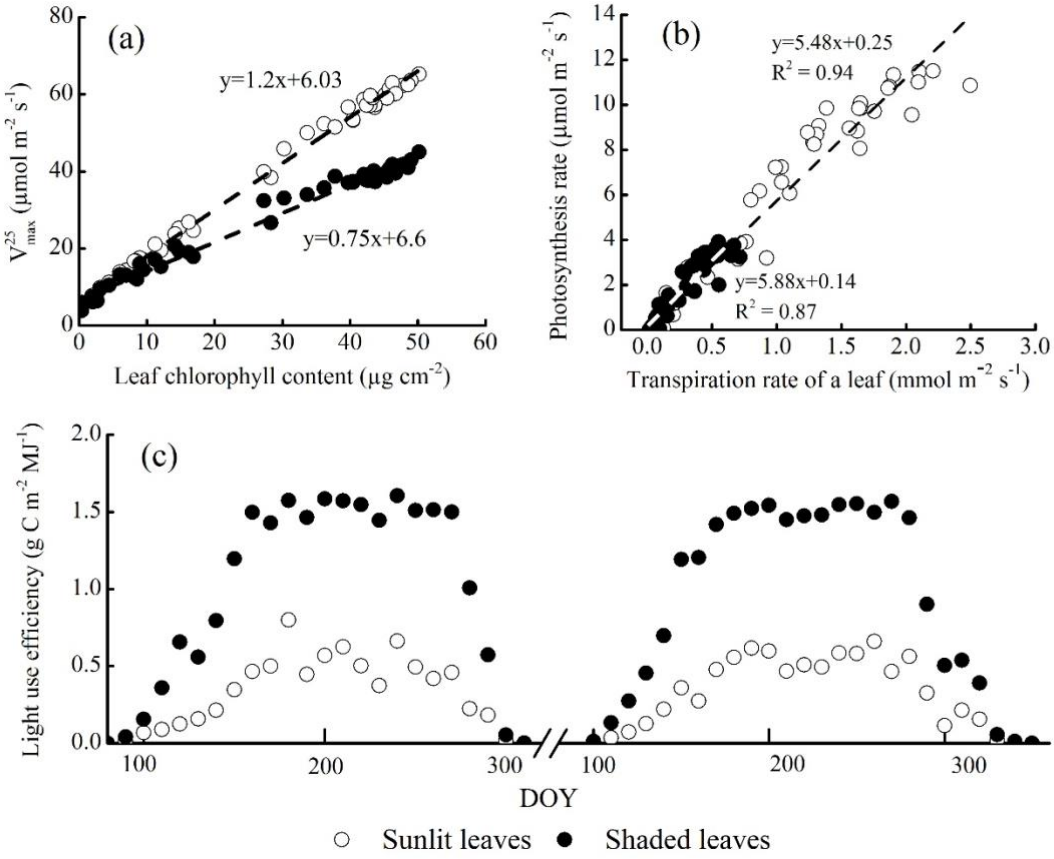

Figure 8. Physiological differences, from BEPS simulations, between sunlit and shaded leaves. (a) V_{max}^{25} versus leaf chlorophyll content; (b) leaf-level photosynthesis versus transpiration; (c) the seasonal variation in LUE.

The seasonal average V_{max}^{25} of a sunlit leaf is 34% higher than that of a shaded leaf, with the biggest difference of 53% occurring in the middle of the growing seasons (Figure 8a). According to our modelling results, the carbon and water fluxes of leaves are strongly coupled, and the water use efficiency (WUE) of the shaded leaf group is similar to that of sunlit leaves (Figure 8b). For an unit area of leaves, 1 mmol of transpired water could incur 5.5 and 5.8

572 μmols of carbon assimilation for sunlit leaves and shaded leaves, respectively. However, light
573 use efficiency (LUE) of leaves fluctuates with Chl_{leaf} (Croft et al., 2015a; Houborg et al., 2011).
574 According to modelled results from BEPS, the LUE of sunlit leaves ranges from 0.02 to 0.62
575 g C m^{-2} MJ^{-1} APAR with an average of 0.35 g m^{-2} MJ^{-1}. Shaded leaves are more efficient in
576 photosynthesis with a LUE ranging from 0.02 to 1.54 g C m^{-2} MJ^{-1}, averaging 1.04 g C m^{-2} MJ^{-1} (Figure 8c). These LUE values are within the range of observed and modelled LUE reported
578 previously reported in the literature (Medlyn, 1998; Yuan et al., 2007). Our finding -- that the
579 modelled LUE of shaded leaves is almost 3 times the modelled LUE of sunlit leaves -- echoes
580 the theory that plants are more capable of utilising diffuse radiation than direct radiation (Gu
581 et al., 2002), since shaded leaves only receive diffuse solar radiation for photosynthesis.
582
583 **4. Discussion**
584 **4.1 Improved seasonal representation for GPP and ET simulations**
585 The comparison of the four modelling cases demonstrates that Chl_{leaf} is the best constraint for
586 V_{max}^{25} in the TBM. Seasonal changes in V_{max}^{25} represent changes in the leaf Rubisco content,
587 which is believed to synchronize with the leaf nitrogen pool (Evans, 1989a). In previous studies,
588 leaf structural parameters such as LAI and SLA were used in models to represent seasonal
589 changes in V_{max}^{25}, assuming that LAI and SLA can provide robust representations of the leaf
590 total nitrogen content. However, the seasonal change in leaf total nitrogen varies from the trend
591 of the leaf photosynthetic nitrogen pool (Croft et al., 2017; Migita et al., 2007; Warren et al.,
592 2000), due to disparity between leaf physiological and morphological development shown in
593 Figure 4 (Croft et al., 2014b). As a consequence, it is important to consider leaf photosynthetic

nitrogen and its relationship to Rubisco content, rather than merely leaf total nitrogen. In this study, we found that Chl_{leaf} can serve as a direct proxy of the leaf photosynthetic nitrogen pool at the canopy top, thus, can constrain the seasonal variation of V_{max}^{25}. The results also suggest that the accumulation and degradation rates for photosynthetic nitrogen pool (as represented by Chl_{leaf}) differ from the rates of changes of leaf and canopy structural components (i.e. LAI and SLA). Consequently, the seasonality of GPP and ET is better explained by Chl_{leaf} than by SLA or LAI, especially during these transitional periods when the disparity between leaf structure and leaf physiology reaches its maximum. In the middle of the growing season, the simulations from four cases are quite similar to each other because leaves were structurally and physiologically mature.

The seasonality of GPP and ET is also influenced by climatic factors. Though carbon and water fluxes are regulated by the stomata (e.g. Baldocchi 1994; Leuning 1990), our sensitivity analysis finds that GPP and ET are not tightly coupled as expected because of their different sensitivities to non-biological factors. Figure 5 demonstrates that Chl_{leaf} was the dominant factor in controlling the carbon uptake, whereas air temperature and atmospheric mositure demand place the strongest controls on water exchange. This finding was also noted in previous sensitivity studies on several TBMs, which also found V_{max}^{25} is a more influential factor for carbon flux modelling than for water flux modelling (Alton et al., 2007; Ryu et al., 2011). Wang and Dickinson (2012) reviewed observational ET studies across the globe and suggested that available energy and vapor pressure deficit are the two most important factors in determining ET in temperate and boreal forest ecosystems like the Borden site. Consequently, it is

reasonable to see that the ET simulations are improved less than the GPP simulations after incorporating Chl_{leaf}-based V_{max}^{25} in the TBM.

4.2 Physiological differences between sunlit and shaded leaves

Many studies have compared the physiological traits of sun and shade-adapted leaves (e.g. Anderson et al., 1988; Boardman, 1977; Chow and Anderson, 1987) and reported that the constituents of photosynthetic components vary with leaf light environments. Under a saturated light environment, leaves tend to assign more nitrogen to produce Rubisco needed in dark reactions of photosynthesis, while shaded leaves will invest more nutrients in the production of the light-harvesting apparatus to capture the photons needed in light reactions. In a canopy, nitrogen is distributed proportionally from top leaves to bottom leaves following the long-term radiation gradient. The sunlit part of the crown tends to have higher N_{area} to produce more photosynthetic components (e.g. Rubisco) in comparison to the shaded part of the canopy. As such, the leaf physiological traits acclimate to leaf light environments to maximize the overall productivity of the whole canopy. Understanding the influence of the light environment on leaves is an important premise before upscaling modelled GPP and ET from leaf to canopy in structurally complex forests.

Estimations from BEPS captures the physiological difference between sunlit and shaded leaves (Figure 7 and 8). With an increase in Chl_{leaf}, V_{max}^{25} and photosynthesis of shaded leaves increase more slowly than those of sunlit leaves, because shaded leaves are predominantly located at the bottom of the canopy where the relatively low nitrogen content constrains the

content of Rubisco. Therefore, the linear relationship between Chl_{leaf} and V_{max}^{25} has a smaller slope for shaded leaves than for sunlit leaves. This finding echoes previous experiments reporting changes in Chl_{leaf} -V_{max}^{25} relationships under different light environments (Table 1).

Table 1. Slopes in the linear Chl_{leaf}–V_{max}^{25} relationships reported in the literatures. Ratios of V_{max}^{25} / Chl_{leaf} in some studies are regarded as slopes. Molecular mass of Chl_{leaf} is 893.5 g mol^{-1}.

Species	Solar irradiance on leaves (μmol m^{-2} s^{-1})	Slopes in Chl_{leaf} –V_{max}^{25} relationships (μmol m^{-2} s^{-1} V_{max}^{25} per μg cm^{-2} Chl_{leaf})	Reference
Cucumis	1000	1.82	(Evans, 1989b) [a]
	550	1.43	
	260	1.43	
	150	1.01	
Phaseolus	820	2.27	
	220	1.58	
	120	1.32	
Maize		1.12	(Houborg et al., 2015b)
Soybean		1.75	
Sorghum		1.25	
Wheat		2.65	
Common bean		1.99	
Cotton		1.76	
Rice		1.60	
Barley		3.07	
Tobacco		2.82	
Deciduous broad leaf tree species	1265 [b]	1.3	This study
Sunlit leaves	972 [c]	1.2	
Shaded leaves	162 [c]	0.77	

[a] J_{max}^{25} is converted into V_{max}^{25} by simply dividing 2;

[b] Measured daytime solar irradiance for leaves on top of the canopy;

[c] The average daytime solar irradiance on leaves, modelled from BEPS, during the period of the growing seasons.

The experimental studies included in Table 1 demonstrate that leaf light environments affect the slopes of Chl_{leaf} –V_{max}^{25} relationships to a degree that is almost comparable to the influence brought by species types. While an increase of 1 μg cm^{-2} in Chl_{leaf} may result in 1 to 3 μmol m^{-2} s^{-1} of increases in V_{max}^{25} for different species, a change in the light environment for a given species could dampen its Chl_{leaf} –V_{max}^{25} slope by a factor between 21% and 44%. Meanwhile, our modelled results show that shaded leaves have a 34% lower Chl_{leaf} –V_{max}^{25} slope than sunlit leaves for deciduous broadleaf trees, which is similar to the results from previous limited experimental studies (Evans, 1989b). Therefore, we suggest that our two-leaf TBM is capable of describing the variations in light environments and is reliable for incorporating Chl_{leaf} in structurally complex forests.

4. Conclusions

Chlorophyll molecules embedded in the light harvesting apparatus are responsible for absorbing solar energy for photosynthesis, and they are also related, through sharing of the leaf nitrogen pool, to the enzyme Rubisco and the cytochrome b6f complex (Cty f) needed by photosynthesis. Based on the key role of chlorophyll in photosynthesis, Chl_{leaf} is regarded as a valuable proxy of the photosynthetic parameters – V_{max}^{25} and J_{max}^{25} – used in TBMs. However, since sun and shade adapted leaves have different strategies in the nitrogen allocation to components of the photosynthetic apparatuses (i.e. chlorophyll and Rubisco), understanding the influence of the light environment on leaves is an important premise before upscaling

modelled GPP and ET from leaf to canopy in the structurally complex forests. In this study, we incorporated a time series of measured Chl_{leaf} into a two-leaf TBM named BEPS. The following conclusions are drawn:

1. Chl_{leaf} provides a reliable constraint on the seasonal variations of V_{max}^{25} and J_{max}^{25} at a forest site. By incorporating Chl_{leaf}–based V_{max}^{25} into BEPS, the biases of simulated annual GPP and annual ET are considerably reduced and the temporal correlations between simulated and measured fluxes are considerably improved relative to three cases using constant V_{max}^{25}, LAI-based V_{max}^{25} and SLA-based V_{max}^{25}. The largest improvements in GPP estimates are witnessed in spring and fall, when MAEs are reduced from between 2.2-3.2 to 1.8 g C m^{-2} d^{-1} and from between 2.1-2.8 to 1.8 g C m^{-2} d^{-1}, respectively. MAEs of modelled ET also shrink from 0.7-0.8 to 0.6 mm d^{-1} in spring while simulated ET does not improve very much in autumn.

2. The two-leaf TBM with V_{max}^{25} constrained by Chl_{leaf} is capable of capturing the physiological differences between sunlit leaves and shaded leaves in a forest stand. According to modelled results, a 1 μg cm^{-2} increase in Chl_{leaf} corresponds to a 1.2 μmols m^{-2} s^{-1} increase in V_{max}^{25} in sunlit leaves and a 0.77 μmols m^{-2} s^{-1} increase in V_{max}^{25} in shaded leaves. The result is in line with the plant physiological studies that found plants optimize the nitrogen allocations to different photosynthetic components according to the light environment to maximize the canopy-scale CO_2 assimilation rate.

This study demonstrates, for the first time, the importance of using chlorophyll in TBMs to reduce the uncertainties in carbon and water flux estimates for forested ecosystems. It also incorporates Chl_{leaf} within a two-leaf scheme to account for the complex light environments inside forest canopies and quantifies the physiological difference between sunlit and shaded

leaves.

Acknowledgement

This study is financially supported by a Discovery Grant and a Strategic Grant from the Natural Science and Engineering Council of Canada. We are very grateful to Prof. Sarah Finkelstein from the University of Toronto for providing the spectrophotometer to help with the chlorophyll measurement.

Appendix A. Net radiation on sunlit and shaded leaves

In every hourly time step of BEPS, the whole canopy was divided into four groups of leaves based on the location and radiation features of the leaves, namely sunlit leaves in the overstorey, shaded leaves in the overstorey, sunlit leaves in the understorey and shaded leaves in the understorey (Chen et al., 1999; Liu et al., 2003). The leaves in each group have identical features so BEPS could use one leaf to represent one group. Net radiation on a leaf is composed by three sources:

$$R_{n\_i} = R_{dir\_i} + R_{dif\_i} + R_{l\_i} \quad \text{(A1)}$$

where R_n is the total net radiation on a certain leaf, R_{dir}, R_{dif} and R_l refers to the net direct incoming solar radiation, net diffuse solar radiation and net longwave radiation on this leaf. *i* refers to one of the four types of leaves. For a shaded leaf, $R_{dir} = 0$.

In order to differentiate the incoming solar radiation into a direct and diffuse part, a semi-empirical equation is applied:

$$\frac{S_{dif}}{S_g} = \begin{cases} 0.943 + 0.734r - 4.9r^2 + 1.796r^3 + 2.058r^4 & r < 0.8 \\ 0.13 & r \geq 0.8 \end{cases} \quad \text{(A2)}$$

$$S_{dir} = S_g - S_{dif} \quad \text{(A3)}$$

where S_g, S_{dir} and S_{dif} are global solar radiation, incoming direct solar radiation and diffuse solar radiation. *r* is a parameter used to quantify the cloudiness in sky

$$r = \frac{S_g}{S_0 cos\theta} \quad \text{(A4)}$$

S_0 is the solar constant set as 1362 W/m2, θ is the solar zenith angel in this hourly time step. The net direct shortwave radiation on the sunlit representative leaf in the overstorey or understorey of the canopy is:

$$R_{dir\_o\_sunlit} = R_{dir\_u\_sunlit} = (1 - \alpha_L) S_{dir} cos\alpha / cos\theta \quad \text{(A5)}$$

where α_L is the albedo of leaves. α is the mean leaf-sun angle which is fixed at 60^o when the canopy has a spherical leaf distribution.

On the other hand, the net diffuse shortwave radiation on the four groups of the leaves are approximated respectively as:

$$R_{dif\_o\_sunlit} = R_{dif\_o\_shaded} = (1 - \alpha_L)\left(S_{dif}\left[1 - e^{-0.5\Omega LAI_o / cos\bar{\theta}_o}\right]/LAI_o + C_o\right) \quad \text{(A6)}$$

$$R_{dif\_u\_sunlit} = R_{dif\_u\_shaded} = (1 - \alpha_L)(S_{dif} e^{-0.5\Omega LAI_o / cos\bar{\theta}_o}\left[1 - e^{-0.5\Omega LAI_u / cos\bar{\theta}_u}\right]/LAI_u + C_u) \quad \text{(A7)}$$

LAI_o and LAI_u denote the LAI value of the overstorey and the understorey, C_o and C_u are used to quantify the multiple scattering of the direct solar radiation from the leaf (Chen et al., 1999)

$$C_o = 0.07\Omega S_{dir}(1.1 - 0.1LAI)e^{-cos\theta} \quad \text{(A8)}$$

$$C_u = 0.07\Omega S_{dir} e^{-0.5\Omega LAI_o / cos\theta}(1.1 - 0.1LAI_u)e^{-cos\theta} \quad \text{(A9)}$$

$\bar{\theta}_o$ and $\bar{\theta}_o$ are the representative zenith angles for diffuse radiation transmission of the overstorey and understorey leaves and slightly dependent on the corresponding LAI (Liu et al.,

2003):

$$cos\bar{\theta} = 0.537 + 0.025LAI \quad \text{(A10)}$$

The net longwave radiation on these leaves is calculated as:

$$R_{L\_o\_sunlit} = R_{L\_o\_shaded} = \frac{1}{LAI_o}\Big\{\{\varepsilon_o[\varepsilon_a\sigma T_a^4 + \varepsilon_u\sigma T_u^4(1 - e^{-0.5LAI_u\Omega/cos\bar{\theta}_u}) + \varepsilon_g\sigma T_g^4 e^{-0.5LAI_u\Omega/cos\bar{\theta}_u}] - 2\varepsilon_o\sigma T_o^4\}(1 - e^{-0.5LAI_o\Omega/cos\bar{\theta}_o}) + \varepsilon_o(1-\varepsilon_u)(1 - e^{-0.5LAI_u\Omega/cos\bar{\theta}_u})[\varepsilon_a\sigma T_a^4 e^{-0.5LAI_o\Omega/cos\bar{\theta}_o} + \varepsilon_o\sigma T_o^4(1 - e^{-0.5LAI_o\Omega/cos\bar{\theta}_o})]\Big\} \quad \text{(A11)}$$

$$R_{L\_u\_sunlit} = R_{L\_u\_shaded} = \frac{1}{LAI_u}\Big\{\{\varepsilon_u[\varepsilon_a\sigma T_a^4 e^{-0.5LAI_o\Omega/cos\bar{\theta}_o} + \varepsilon_o\sigma T_o^4(1 - e^{-0.5LAI_o\Omega/cos\bar{\theta}_o}) + \varepsilon_g\sigma T_g^4] - 2\varepsilon_u\sigma T_u^4\}(1 - e^{-0.5LAI_u\Omega/cos\bar{\theta_u}}) + \varepsilon_u(1-\varepsilon_g)\{[\varepsilon_a\sigma T_a^4 e^{-0.5LAI_o\Omega/cos\bar{\theta}_o} + \varepsilon_o\sigma T_o^4(1 - e^{-0.5LAI_o\Omega/cos\bar{\theta}_o})]e^{-0.5LAI_u\Omega/cos\bar{\theta}_u} + \varepsilon_u\sigma T_u^4(1 - e^{-0.5LAI_u\Omega/cos\bar{\theta}_u})\} + \varepsilon_u(1-\varepsilon_o)[\varepsilon_u\sigma T_u^4(1 - e^{-0.5LAI_u\Omega/cos\bar{\theta}_u}) + \varepsilon_g\sigma T_g^4 e^{-0.5LAI_u\Omega/cos\bar{\theta}_u}](1 - e^{-0.5LAI_o\Omega/cos\bar{\theta}_o})\Big\} \quad \text{(A12)}$$

where σ is the Stephen-Boltzmann constant equals to $5.67 \times 10^{-8} Wm^{-2}K^{-4}$. ε_a, ε_o, ε_u and ε_g are the emissivity of the atmosphere, overstory, understory and ground surface, respectively. ε_o, ε_u and ε_g are prescribed as 0.98, 0.98 and 0.95 according to (Chen and Zhang, 1989; Chen et al., 1989), and ε_a is computed as $\varepsilon_a = 1.24(\frac{e_a}{T_a})^{1/7}$(Brutsaert, 1982), where e_a and T_a are water vapor pressure in *mbar* and temperature of the atmosphere in *K*. T_o, T_u and T_g are the temperatures of the overstory, the understorey and ground in *K*.

Appendix B. Quantification of the soil water stress factor

To assess the effect of soil water deficit on stomatal conductance (*fw*), a scaling factor based on the ratio of the real time available water in soil to the maximum plant available water (Chen

et al., 2005; Wang and Leuning, 1998; Wigmosta et al., 1994) is used to implement the soil water information.

$$fw = \begin{cases} 0 & \theta_{sw}(z) < \theta_{wp} \\ \frac{\theta_{sw}(z) - \theta_{wp}}{\theta_{fc} - \theta_{wp}} & \theta_{wp} \le \theta_{sw}(z) \le \theta_{fc} \\ 1 & \theta_{sw}(z) > \theta_{fc} \end{cases} \quad \text{(B1)}$$

where $\theta_{sw}(z)$ is the soil water content of layer z, z often refers to the top 30 cm based on the availability of the soil water measurements. θ_{wp} and θ_{fc} are the wilting point and the field capacity (m_3/m_3) of the soil layer. θ_{wp} and θ_{fc} are derived by the soil texture information provided on the Fluxnet archive (http://fluxnet.ornl.gov/), the patterns of multi-year soil moisture measurements and the algorithm developed by Saxton and Rawls (2006).

Reference

Alton, P., Mercado, L., North, P., 2007. A sensitivity analysis of the land-surface scheme JULES conducted for three forest biomes: Biophysical parameters, model processes, and meteorological driving data, Global Biogeochemical Cycles, 20, GB1008, doi:10.1029/2005GB002653.

Alton, P., 2017. Retrieval of seasonal Rubisco-limited photosynthetic capacity at global FLUXNET sites from hyperspectral satellite remote sensing: Impact on carbon modelling, Agricultural and Forest Meteorology, 232, 74-88, http://doi.org/10.1016/j.agrformet.2016.08.001.

Amthor, J.S., Chen, J.M., Clein, J.S., Frolking, S.E., Goulden, M.L., Grant, R.F., Kimball, J.S., King, A.W., McGuire, A.D., Nikolov, N.T., Potter, C.S., Wang, S., Wofsy, S.C., 2001. Boreal forest CO 2 exchange and evapotranspiration predicted by nine ecosystem process models: Intermodel comparisons and relationships to field measurements. Journal of Geophysical Research 106, 33623. doi:10.1029/2000JD900850

Anderson, J., Chow, W., Goodchild, D., 1988. Thylakoid Membrane Organisation in Sun/Shade Acclimation. Australian Journal of Plant Physiology 15, 11. doi:10.1071/PP9880011

Baldocchi, D., 1994. An analytical solution for coupled leaf photosynthesis and stomatal conductance models, Tree Physiology, 14, 1069–1079, doi:10.1093/treephys/14.7-8-9.1069.

Barr, A.G., Black, T.A., Hogg, E.H., Kljun, N., Morgenstern, K., Nesic, Z., 2004. Inter-annual variability in the leaf area index of a boreal aspen-hazelnut forest in relation to net ecosystem production. Agricultural and Forest Meteorology 126, 237–255. doi:10.1016/j.agrformet.2004.06.011

790 Barr, A.G., Richardson, A.D., Hollinger, D.Y., Papale, D., Arain, M.A., Black, T.A., et al., 2013.
791 Use of change-point detection for friction–velocity threshold evaluation in eddy-
792 covariance studies. Agric. For. Meteorol. 171–172, 31–45.

793 Boardman, N.K., 1977. Comparative Photosynthesis of Sun and Shade Plants. Annual Review
794 of Plant Physiology 28, 355–377. doi:10.1146/annurev.pp.28.060177.002035

795 Brutsaert, W., 1982. Evaporation into the Atmosphere. Springer Netherlands, Dordrecht.
796 doi:10.1007/978-94-017-1497-6

797 Chen, B., Chen, J.M., Ju, W., 2007. Remote sensing-based ecosystem-atmosphere simulation
798 scheme (EASS)-Model formulation and test with multiple-year data. Ecological
799 Modelling 209, 277–300. doi:10.1016/j.ecolmodel.2007.06.032

800 Chen, B., Liu, J., Chen, J.M., Croft, H., Gonsamo, A., He, L., Luo, X., 2016. Assessment of
801 foliage clumping effects on evapotranspiration estimates in forested ecosystems,
802 Agricultural and Forest Meteorology, 216, 82-92.

803 Chen, J.M., Zhang, R.H., 1989. Studies on the measurements of crop emissivity and sky
804 temperature. Agricultural and Forest Meteorology 49, 23–34. doi:10.1016/0168-
805 1923(89)90059-2

806 Chen, J.., Liu, J., Cihlar, J., Goulden, M.., 1999. Daily canopy photosynthesis model through
807 temporal and spatial scaling for remote sensing applications. Ecological Modelling 124,
808 99–119. doi:10.1016/S0304-3800(99)00156-8

809 Chen, J.M., Chen, X., Ju, W., Geng, X., 2005. Distributed hydrological model for mapping
810 evapotranspiration using remote sensing inputs. Journal of Hydrology 305, 15–39.
811 doi:10.1016/j.jhydrol.2004.08.029

812 Chen, J.M., Cihlar, J., 1995. Plant canopy gap-size analysis theory for improving optical
813 measurements of leaf-area index. Applied optics 34, 6211–6222.
814 doi:10.1364/AO.34.006211

815 Chen, J.M., Mo, G., Pisek, J., Liu, J., Deng, F., Ishizawa, M., Chan, D., 2012. Effects of foliage
816 clumping on the estimation of global terrestrial gross primary productivity. Global
817 Biogeochemical Cycles 26, 1–18. doi:10.1029/2010GB003996

818 Chen, J.M., Yang, B.J., Zhang, R.H., 1989. Soil thermal emissivity as affected by its water
819 content and surface treatment. Soil science (USA).

820 Chow, W.S., Anderson, J.M., 1987. Photosynthetic responses of Pisum sativum to an increase
821 in irradiance during growth. II. Thylakoid membrane components. Functional Plant
822 Biology 14, 9–19. doi:doi:10.1071/PP9870009

823 Croft, H., Chen, J.M., Froelich, N.J., Chen, B., Staebler, R.M., 2015a. Seasonal controls of
824 canopy chlorophyll content on forest carbon uptake: Implications for GPP modeling.
825 Journal of Geophysical Research: Biogeosciences 120, n/a-n/a.
826 doi:10.1002/2015JG002980

827 Croft, H., Chen, J.M., Luo, X., Barlett, P., Chen, B., Staebler, R.M., n.d. Leaf chlorophyll

content as a proxy for leaf photosynthetic capacity. Global Change Biology.

Croft, H., Chen, J.M., Zhang, Y., 2014a. The applicability of empirical vegetation indices for determining leaf chlorophyll content over different leaf and canopy structures. Ecological Complexity 17, 119–130. doi:10.1016/j.ecocom.2013.11.005

Croft, H., Chen, J.M., Zhang, Y., 2014b. Temporal disparity in leaf chlorophyll content and leaf area index across a growing season in a temperate deciduous forest. International Journal of Applied Earth Observation and Geoinformation 33, 312–320. doi:10.1016/j.jag.2014.06.005

Croft, H., Chen, J.M., Zhang, Y., Simic, A., 2013. Modelling leaf chlorophyll content in broadleaf and needle leaf canopies from ground, CASI, Landsat TM 5 and MERIS reflectance data. Remote Sensing of Environment 133, 128–140. doi:10.1016/j.rse.2013.02.006

Croft, H., Chen, J.M., Zhang, Y., Simic, A., Noland, T.L., Nesbitt, N., Arabian, J., 2015b. Evaluating leaf chlorophyll content prediction from multispectral remote sensing data within a physically-based modelling framework. ISPRS Journal of Photogrammetry and Remote Sensing 102, 85–95. doi:10.1016/j.isprsjprs.2015.01.008

De Pury, D.G.G., Farquhar, G.D., 1997. Simple scaling of photosynthesis from leaves to canopies without the errors of big-leaf models. Plant, Cell and Environment 20, 537–557. doi:10.1111/j.1365-3040.1997.00094.x

Demarez, V., Gastellu-Etchegorry, J.P., Mogin, E., Marty, G., Proisy, C., Dufréne, E., Dantec, V. Le, 1999. Seasonal variation of leaf chlorophyll content of a temperate forest. Inversion of the PROSPECT model. International Journal of Remote Sensing 20, 879–894.

Ethier, G.J., Livingston, N.J., 2004. On the need to incorporate sensitivity to CO2 transfer conductance into the Farquhar-von Caemmerer-Berry leaf photosynthesis model. Plant, Cell and Environment 27, 137–153. doi:10.1111/j.1365-3040.2004.01140.x

Evans, J., 1989a. Photosynthesis and nitrogen relationships in leaves of C3 plants. Oecologia 78, 9–19. doi:10.1007/BF00377192

Evans, J., 1989b. Partitioning of Nitrogen Between and Within Leaves Grown Under Different Irradiances. Australian Journal of Plant Physiology 16, 533. doi:10.1071/PP9890533

Farquhar, G.D., von Caemmerer, S., Berry, J.A., 1980. A biochemical model of photosynthetic CO2 assimilation in leaves of C 3 species. Planta 149, 78–90. doi:10.1007/BF00386231

Field, C., 1983. Allocating leaf nitrogen for the maximization of carbon gain: Leaf age as a control on the allocation program. Oecologia 56, 341–347. doi:10.1007/BF00379710

Froelich, N., Croft, H., Chen, J.M., Gonsamo, A., Staebler, R.M., 2015. Trends of carbon fluxes and climate over a mixed temperate–boreal transition forest in southern Ontario, Canada. Agricultural and Forest Meteorology 211–212, 72–84. doi:10.1016/j.agrformet.2015.05.009

Gitelson, A.A., Viña, A., Ciganda, V., Rundquist, D.C., Arkebauer, T.J., 2005. Remote

866 estimation of canopy chlorophyll content in crops. Geophysical Research Letters 32,
867 L08403. doi:10.1029/2005GL022688

868 Gitelson, A.A., Viña, A., Verma, S.B., Rundquist, D.C., Arkebauer, T.J., Keydan, G., Leavitt,
869 B., Ciganda, V., Burba, G.G., Suyker, A.E., 2006. Relationship between gross primary
870 production and chlorophyll content in crops: Implications for the synoptic monitoring of
871 vegetation productivity. Journal of Geophysical Research Atmospheres 111, 1–13.
872 doi:10.1029/2005JD006017

873 Gonsamo, A., Chen, J.M., Price, D.T., Kurz, W. a., Liu, J., Boisvenue, C., Hember, R. a., Wu,
874 C., Chang, K.H., 2013. Improved assessment of gross and net primary productivity of
875 Canada's landmass. Journal of Geophysical Research: Biogeosciences 118, 1546–1560.
876 doi:10.1002/2013JG002388

877 Gonsamo, A., Croft, H., Chen, J.M., Wu, C., Froelich, N., Staebler, R.M., 2015. Radiation
878 contributed more than temperature to increased decadal autumn and annual carbon uptake
879 of two eastern North America mature forests. Agricultural and Forest Meteorology 201,
880 8–16. doi:10.1016/j.agrformet.2014.11.007

881 Grant, R.F., Zhang, Y., Yuan, F., Wang, S., Hanson, P.J., Gaumont-Guay, D., Chen, J., Black, T.
882 a., Barr, a., Baldocchi, D.D., Arain, a., 2006. Intercomparison of techniques to model
883 water stress effects on CO2 and energy exchange in temperate and boreal deciduous
884 forests. Ecological Modelling 196, 289–312. doi:10.1016/j.ecolmodel.2006.02.035

885 Groenendijk, M., Dolman, A.J., Ammann, C., Arneth, A., Cescatti, A., Dragoni, D., Gash,
886 J.H.C., Gianelle, D., Gioli, B., Kiely, G., Knohl, A., Law, B.E., Lund, M., Marcolla, B.,
887 van der Molen, M.K., Montagnani, L., Moors, E., Richardson, A.D., Roupsard, O.,
888 Verbeeck, H., Wohlfahrt, G., 2011. Seasonal variation of photosynthetic model parameters
889 and leaf area index from global Fluxnet eddy covariance data. Journal of Geophysical
890 Research 116, G04027. doi:10.1029/2011JG001742

891 Gu, L., Baldocchi, D., Verma, S.B., Black, T.A., Vesala, T., Falge, E.M., Dowty, P.R., 2002.
892 Advantages of diffuse radiation for terrestrial ecosystem productivity. Journal of
893 Geophysical Research: Atmospheres 107, ACL 2-1. doi:10.1029/2001JD001242

894 Hikosaka, K., 2014. Optimal nitrogen distribution within a leaf canopy under direct and diffuse
895 light. Plant, cell & environment 37, 2077–85. doi:10.1111/pce.12291

896 Hikosaka, K., Terashima, I., 1996. Nitrogen partitioning among photosynthetic components
897 and its consequenses in sun and shade plants. Functional Ecology 10, 335–343.
898 doi:10.2307/2390281

899 Hikosaka, K., Terashima, I., 1995. A model of the acclimation of photosynthesis in the leaves
900 of C3 plants to sun and shade with respect to nitrogen use. Plant, Cell and Environment
901 18, 605–618. doi:10.1111/j.1365-3040.1995.tb00562.x

902 Hirose, T., Werger, M.J. a, 1987. Maximizing dialy canopy phoytosynthesis with respect to the
903 leaf nitrogen allocation pattern in the canopy. Oecologia 72, 520–526.
904 doi:10.1007/BF00378977

905 Houborg, R., Anderson, M.C., Daughtry, C.S.T., Kustas, W.P., Rodell, M., 2011. Using leaf
906 chlorophyll to parameterize light-use-efficiency within a thermal-based carbon, water and
907 energy exchange model. Remote Sensing of Environment 115, 1694–1705.
908 doi:10.1016/j.rse.2011.02.027

909 Houborg, R., Cescatti, A., Migliavacca, M., Kustas, W.P., 2013. Satellite retrievals of leaf
910 chlorophyll and photosynthetic capacity for improved modeling of GPP. Agricultural and
911 Forest Meteorology 177, 10–23. doi:10.1016/j.agrformet.2013.04.006

912 Houborg, R., McCabe, M., Cescatti, A., Gao, F., Schull, M., Gitelson, A., 2015a. Joint leaf
913 chlorophyll content and leaf area index retrieval from Landsat data using a regularized
914 model inversion system (REGFLEC). Remote Sensing of Environment 159, 203–221.
915 doi:10.1016/j.rse.2014.12.008

916 Houborg, R., McCabe, M.F., Cescatti, A., Gitelson, A.A., 2015b. Leaf chlorophyll constraint
917 on model simulated gross primary productivity in agricultural systems. International
918 Journal of Applied Earth Observation and Geoinformation 43, 160–176.
919 doi:10.1016/j.jag.2015.03.016

920 Iio, A., Fukasawa, H., Nose, Y., Kato, S., Kakubari, Y., 2005. Vertical, horizontal and azimuthal
921 variations in leaf photosynthetic characteristics within a Fagus crenata crown in relation
922 to light acclimation. Tree physiology 25, 533–544. doi:10.1093/treephys/25.5.533

923 Ju, W., Chen, J.M., Black, T.A., Barr, A.G., Liu, J., Chen, B., 2006. Modelling multi-year
924 coupled carbon and water fluxes in a boreal aspen forest. Agricultural and Forest
925 Meteorology 140, 136–151. doi:10.1016/j.agrformet.2006.08.008

926 Jung, M., Reichstein, M., Ciais, P., Seneviratne, S.I., Sheffield, J., Goulden, M.L., Bonan, G.,
927 Cescatti, A., Chen, J., de Jeu, R., Dolman, a J., Eugster, W., Gerten, D., Gianelle, D.,
928 Gobron, N., Heinke, J., Kimball, J., Law, B.E., Montagnani, L., Mu, Q., Mueller, B.,
929 Oleson, K., Papale, D., Richardson, A.D., Roupsard, O., Running, S., Tomelleri, E., Viovy,
930 N., Weber, U., Williams, C., Wood, E., Zaehle, S., Zhang, K., 2010. Recent decline in the
931 global land evapotranspiration trend due to limited moisture supply. Nature 467, 951–954.
932 doi:10.1038/nature09396

933 Kalacska, M., Lalonde, M., Moore, T.R., 2015. Estimation of foliar chlorophyll and nitrogen
934 content in an ombrotrophic bog from hyperspectral data: Scaling from leaf to image.
935 Remote Sensing of Environment 169, 270–279. doi:10.1016/j.rse.2015.08.012

936 Kattge, J., Knorr, W., Raddatz, T., Wirth, C., 2009. Quantifying photosynthetic capacity and its
937 relationship to leaf nitrogen content for global-scale terrestrial biosphere models. Global
938 Change Biology 15, 976–991. doi:10.1111/j.1365-2486.2008.01744.x

939 Knyazikhin, Y., Schull, M.A., Stenberg, P., Mõttus, M., Rautiainen, M., Yang, Y., Marshak, A.,
940 Latorre Carmona, P., Kaufmann, R.K., Lewis, P., Disney, M.I., Vanderbilt, V., Davis, A.B.,
941 Baret, F., Jacquemoud, S., Lyapustin, A., Myneni, R.B., 2013. Hyperspectral remote
942 sensing of foliar nitrogen content. Proceedings of the National Academy of Sciences of
943 the United States of America 110, E185-92. doi:10.1073/pnas.1210196109

944 Koffi, E.N., Rayner, P.J., Norton, A.J., Frankenberg, C., and Scholze, M., 2015. Investigating

945 the usefulness of satellite-derived fluorescence data in inferring gross primary
946 productivity within the carbon cycle data assimilation system, Biogeosciences, 12, 4067-
947 4084, doi:10.5194/bg-12-4067-2015

948 Kull, O., 2002. Acclimation of photosynthesis in canopies: models and limitations. Oecologia
949 133, 267–279. doi:10.1007/s00442-002-1042-1

950 Lambers, H., Chapin, F.S., Pons, T.L., 2008. Plant Physiological Ecology. Springer New York,
951 New York, NY. doi:10.1007/978-0-387-78341-3

952 Lee, X., Fuentes, J.D., Staebler, R.M., Neumann, H.H., 1999. Long-term observation of the
953 atmospheric exchange of CO 2 with a temperate deciduous forest in southern Ontario,
954 Canada. Journal of Geophysical Research 104, 15975. doi:10.1029/1999JD900227

955 Leuning, R., 1990. Modelling Stomatal Behaviour and and Photosynthesis of Eucalyptus
956 grandis, Australian Journal of Plant Physiology, 17, 159–175, doi:10.1071/PP9900159.

957 Lichtenthaler, H.K., Ač, A., Marek, M. V., Kalina, J., Urban, O., 2007. Differences in pigment
958 composition, photosynthetic rates and chlorophyll fluorescence images of sun and shade
959 leaves of four tree species. Plant Physiology and Biochemistry 45, 577–588.
960 doi:10.1016/j.plaphy.2007.04.006

961 Liu, J., Chen, J.M., Cihlar, J., 2003. Mapping evapotranspiration based on remote sensing: An
962 application to Canada's landmass. Water Resources Research 39.
963 doi:10.1029/2002WR001680

964 Luo, X., Chen, J.M., Liu, J., Black, T.A., Croft, H., Staebler, R., He, L., Arain, M.A., Chen, B.,
965 Mo, G., Gonsamo, A., McCaughey, H., 2017. Comparing big-leaf scheme, two-big-leaf
966 scheme and two-leaf scheme for evapotranspiration estimation through coupled carbon-
967 water modelling. Water Resources Research, in review.

968 Medlyn, B.E., 1998. Physiological basis of the light use efficiency model. Tree Physiology 18,
969 167–176. doi:10.1093/treephys/18.3.167

970 Medlyn, B.E., Badeck, F.-W., De Pury, D.G.G., Barton, C.V.M., Broadmeadow, M., Ceulemans,
971 R., De Angelis, P., Forstreuter, M., Jach, M.E., Kellomäki, S., Laitat, E., Marek, M.,
972 Philippot, S., Rey, A., Strassemeyer, J., Laitinen, K., Liozon, R., Portier, B., Roberntz, P.,
973 Wang, K., Jstbid, P.G., 1999. Effects of elevated [CO2] on photosynthesis in European
974 forest species: a meta-analysis of model parameters. Plant, Cell & Environment 22, 1475–
975 1495. doi:10.1046/j.1365-3040.1999.00523.x

976 Niinemets, U., 1997. Acclimation to low irradiance in Picea abies: influences of past and
977 present light climate on foliage structure and function. Tree physiology 17, 723–32.
978 doi:10.1093/treephys/17.11.723

979 Norman, J.M., 1982. Biometeorology in Integrated Pest Management, Biometeorology in
980 Integrated Pest Management. Elsevier. doi:10.1016/B978-0-12-332850-2.50009-8

981 Oki, T., Kanae, S., 2006. Global hydrological cycles and world water resources. Science (New
982 York, N.Y.) 313, 1068–1072. doi:10.1126/science.1128845

983 Pan, Y., Birdsey, R.A., Phillips, O.L., Jackson, R.B., 2013. The Structure, Distribution, and
984 Biomass of the World's Forests. Annual Review of Ecology, Evolution, and Systematics
985 44, 593–622. doi:10.1146/annurev-ecolsys-110512-135914

986 Porcar-Castell, A., Tyystjärvi, E., Atherton, J., Van Der Tol, C., Flexas, J., Pfündel, E.E.,
987 Moreno, J., Frankenberg, C., Berry, J.A., 2014. Linking chlorophyll a fluorescence to
988 photosynthesis for remote sensing applications: Mechanisms and challenges. Journal of
989 Experimental Botany 65, 4065–4095. doi:10.1093/jxb/eru191

990 Potter, C.S., Wang, S., Nikolov, N.T., McGuire, A.D., Liu, J., King, A.W., Kimball, J.S., Grant,
991 R.F., Frolking, S.E., Clein, J.S., Chen, J.M., Amthor, J.S., 2001. Comparison of boreal
992 ecosystem model sensitivity to variability in climate and forest site parameters. Journal of
993 Geophysical Research 106, 33671. doi:10.1029/2000JD000224

994 Ryu, Y., Baldocchi, D.D., Kobayashi, H., van Ingen, C., Li, J., Black, T.A., Beringer, J., van
995 Gorsel, E., Knohl, A., Law, B.E., Roupsard, O., 2011. Integration of MODIS land and
996 atmosphere products with a coupled-process model to estimate gross primary productivity
997 and evapotranspiration from 1 km to global scales. Global Biogeochemical Cycles 25,
998 n/a-n/a. doi:10.1029/2011GB004053

999 Sage, R.F., Pearcy, R.W., Seemann, J.R., 1987. The Nitrogen Use Efficiency of C(3) and C(4)
1000 Plants : III. Leaf Nitrogen Effects on the Activity of Carboxylating Enzymes in
1001 Chenopodium album (L.) and Amaranthus retroflexus (L.). Plant physiology 85, 355–9.

1002 Saxton, K.E., Rawls, W.J., 2006. Soil Water Characteristic Estimates by Texture and Organic
1003 Matter for Hydrologic Solutions. Soil Science Society of America Journal 70, 1569.
1004 doi:10.2136/sssaj2005.0117

1005 Schaefer, K., Schwalm, C.R., Williams, C., Arain, M.A., Barr, A., Chen, J.M., Davis, K.J.,
1006 Dimitrov, D., Hilton, T.W., Hollinger, D.Y., Humphreys, E., Poulter, B., Raczka, B.M.,
1007 Richardson, A.D., Sahoo, A., Thornton, P., Vargas, R., Verbeeck, H., Anderson, R., Baker,
1008 I., Black, T.A., Bolstad, P., Chen, J., Curtis, P.S., Desai, A.R., Dietze, M., Dragoni, D.,
1009 Gough, C., Grant, R.F., Gu, L., Jain, A., Kucharik, C., Law, B., Liu, S., Lokipitiya, E.,
1010 Margolis, H.A., Matamala, R., McCaughey, J.H., Monson, R., Munger, J.W., Oechel, W.,
1011 Peng, C., Price, D.T., Ricciuto, D., Riley, W.J., Roulet, N., Tian, H., Tonitto, C., Torn, M.,
1012 Weng, E., Zhou, X., 2012. A model-data comparison of gross primary productivity:
1013 Results from the North American Carbon Program site synthesis. Journal of Geophysical
1014 Research 117, G03010. doi:10.1029/2012JG001960

1015 Sharkey, T.D., Bernacchi, C.J., Farquhar, G.D., Singsaas, E.L., 2007. Fitting photosynthetic
1016 carbon dioxide response curves for C3 leaves. Plant, Cell and Environment 30, 1035–
1017 1040. doi:10.1111/j.1365-3040.2007.01710.x

1018 Sinclair, T.R., Murphy, C.E., Knoerr, K.R., 1976. Development and Evaluation of Simplified
1019 Models for Simulating Canopy Photosynthesis and Transpiration. Journal of Applied
1020 Ecology 13, 813–829.

1021 Staebler, R.M., Fitzjarrald, D.R., 2004. Observing subcanopy CO2 advection. Agricultural and
1022 Forest Meteorology 122, 139–156. doi:10.1016/j.agrformet.2003.09.011

Teklemariam, T., Staebler, R.M., Barr, A.G., 2009. Eight years of carbon dioxide exchange above a mixed forest at Borden, Ontario. Agricultural and Forest Meteorology 149, 2040–2053. doi:10.1016/j.agrformet.2009.07.011

Terashima, I., Evans, J., 1988. Effects of light and nitrogen nutrition on the organization of the photosynthetic apparatus in spinach. Plant and Cell Physiology 29, 143–155.

Thornton, P.E., Zimmermann, N.E., 2007. An improved canopy integration scheme for a Land Surface Model with prognostic canopy structure. Journal of Climate 20, 3902–3923. doi:10.1175/JCLI4222.1

Walker, A.P., Beckerman, A.P., Gu, L., Kattge, J., Cernusak, L.A., Domingues, T.F., Scales, J.C., Wohlfahrt, G., Wullschleger, S.D., Woodward, F.I., 2014. The relationship of leaf photosynthetic traits - V cmax and J max - to leaf nitrogen, leaf phosphorus, and specific leaf area: a meta-analysis and modeling study. Ecology and evolution 4, 3218–35. doi:10.1002/ece3.1173

Walters, R.G., 2005. Towards an understanding of photosynthetic acclimation. Journal of experimental botany 56, 435–47. doi:10.1093/jxb/eri060

Wang, K., Dickinson, R. E., 2012. A review of global terrestrial evapotranspiration: observation, modelling, climatology, and climatic variability, Review of Geophysics, 50(2011), 1–54

Wang, Y.-P., Leuning, R., 1998. A two-leaf model for canopy conductance, photosynthesis and partitioning of available energy I: Agricultural and Forest Meteorology 91, 89–111. doi:10.1016/S0168-1923(98)00061-6

Warren, C.R., Adams, M.A., 2001. Distribution of N, Rubisco and photosynthesis in Pinus pinaster and acclimation to light. Plant, Cell and Environment 24, 597–609. doi:10.1046/j.1365-3040.2001.00711.x

Webb, E.K., Pearman, G.I., Leuning, R., 1980. Correction of flux measurements for density effects due to heat and water vapour transfer. Quarterly Journal of the Royal Meteorological Society 106, 85–100. doi:10.1002/qj.49710644707

Wellburn, A. R. 1994. The spectral determination of chlorophylls a and b, as well as total carotenoids, using various solvents with spectrophotometers of different resolution, Journal of Plant Physiology, 144, 307–313.

Wigmosta, M.S., Vail, L.W., Lettenmaier, D.P., 1994. A distributed hydrology-vegetation model for complex terrain. Water Resources Research 30, 1665–1679. doi:10.1029/94WR00436

Wilson, K.B., Baldocchi, D.D., Hanson, P.J., 2000. Spatial and seasonal variability of photosynthetic parameters and their relationship to leaf nitrogen in a deciduous forest. Tree Physiology 20, 565–578. doi:10.1093/treephys/20.9.565

Wu, C., Niu, Z., Tang, Q., Huang, W., 2008. Estimating chlorophyll content from hyperspectral vegetation indices: Modeling and validation. Agricultural and Forest Meteorology 148, 1230–1241. doi:10.1016/j.agrformet.2008.03.005

Wullschleger, S.D., 1993. Biochemical Limitations to Carbon Assimilation in C 3 Plants—A Retrospective Analysis of the A/C i Curves from 109 Species. Journal of Experimental Botany 44, 907–920. doi:10.1093/jxb/44.5.907

Xu, L., Baldocchi, D.D., 2003. Seasonal trends in photosynthetic parameters and stomatal conductance of blue oak (Quercus douglasii) under prolonged summer drought and high temperature. Tree Physiology 23, 865–877. doi:10.1093/treephys/23.13.865

Yang, X., Tang, J., Mustard, J.F., Wu, J., Zhao, K., Serbin, S., Lee, J.E., 2016. Seasonal variability of multiple leaf traits captured by leaf spectroscopy at two temperate deciduous forests. Remote Sensing of Environment 179, 1–12. doi:10.1016/j.rse.2016.03.026

Yuan, W., Liu, S., Zhou, G., Zhou, G., Tieszen, L.L., Baldocchi, D., Bernhofer, C., Gholz, H., Goldstein, A.H., Goulden, M.L., Hollinger, D.Y., Hu, Y., Law, B.E., Stoy, P.C., Vesala, T., Wofsy, S.C., 2007. Deriving a light use efficiency model from eddy covariance flux data for predicting daily gross primary production across biomes. Agricultural and Forest Meteorology 143, 189–207. doi:10.1016/j.agrformet.2006.12.001

Zhang, Y., Chen, J.M., Thomas, S.C., 2007. Retrieving seasonal variation in chlorophyll content of overstory and understory sugar maple leaves from leaf-level hyperspectral data. Canadian Journal of Remote Sensing 33, 406–415. doi:10.5589/m07-037